Left Ventricular Flow Patterns after Percutaneous Edge-to-Edge Mitral Valve Repair: An *in vitro* Study

Morteza Jeyhani

A Thesis
in
the Department
of
Mechanical and Industrial Engineering

Presented in Partial Fulfilment of the Requirements
for the Degree of Master of Applied Science (Mechanical Engineering) at
Concordia University
Montreal, Quebec, Canada

November 2013

CONCORDIA UNIVERSITY

School of Graduate Studies

This is to certify that the thesis prepared,

By: **Morteza Jeyhani**

Entitled: "**Left Ventricular Flow Patterns after Percutaneous Edge-to-Edge Mitral Valve Repair: An in vitro Study**"

and submitted in partial fulfillment of the requirements for the degree of

Master of Applied Science (Mechanical Engineering)

complies with the regulations of the University and meets the accepted standards with respect to originality and quality.

Signed by the Final Examining Committee:

_____ Chair
Dr. Ali Akgunduz

_____ Examiner
Dr. H.D. Ng

_____ Examiner
Dr. N. Bouguila CIISE External

_____ Supervisor
Dr. Lyes Kadem

Approved by: _____
Dr. Sivakumar Narayanswamy, MASc Program Director
Department of Mechanical and Industrial Engineering

_____
Dean Paula Wood-Adams
Faculty of Engineering and Computer Science

Date: _____

ABSTRACT

Left Ventricular Flow Patterns after Percutaneous Edge-to-Edge Mitral Valve Repair: An *in vitro* Study

Morteza Jeyhani

Percutaneous mitral valve edge-to-edge repair is a viable solution in high-risk patients with severe symptomatic mitral regurgitation. However, the generated double-orifice configuration poses challenges for the evaluation of the hemodynamic performance of the mitral valve and may alter flow patterns in the left ventricle during diastole. The purpose of the present *in vitro* study is to provide new insight into the spatial-temporal hemodynamics of the flow distal to simulated percutaneous edge-to-edge repair by employing a high resolution, flow diagnostic method, Phase Locked and Time Resolved Digital Particle Image Velocimetry inside the LV.

A custom-made mitral valve was developed and two configurations were tested: a single orifice valve with mitral regurgitation and a double-orifice mitral valve configuration. The hemodynamic performance of the valve was evaluated using Doppler echocardiography and catheterization. The flow patterns in the left ventricle were investigated using Particle Image Velocimetry.

Edge-to-edge repair significantly reduced the regurgitant volume. There was a good agreement between Doppler and catheter transmitral pressure gradients. There was a

good match between maximal velocity measured by Doppler and particle image velocimetry. Vortex development in the left ventricle during diastole was significantly different after repair.

There was a good agreement between Doppler and catheter measurements of transmitral pressure gradient following simulated edge-to-edge repair. Flow in the left ventricle was significantly altered by the repair and led to higher energy dissipation during diastole.

This work is dedicated to my parents for being my first and greatest teachers and to my fiancée because of her unconditional and perpetual love and support.

Acknowledgments

I would like to express my gratitude to Dr. Lyes Kadem, my supervisor, for his guidance and help throughout my thesis. I have learned so much during this experience and I thank you for that. I appreciate your passion for research and for challenging me to grow every step of the way and transcend to the next level. Lyes has been supportive of my ideas and has given me appreciated freedom during my work. Thank you for your support.

Besides my advisor, I also wish to express my sincere thanks to Dr. Shahrokh Shahriari whose advices and insight were invaluable to me. For all I learned from him, for his continuing support and moreover his friendship is much appreciated.

In addition, I am grateful to Dr. Michel Labrosse, Department of Mechanical Engineering from University of Ottawa for his contribution to this work.

I would like to acknowledge the members of my thesis committee, who critically reviewed this manuscript and helped me to improve its content and presentation: Dr. Hoi Dick Ng, Dr. Ali Akgunduz and Dr. Nizar Bouguila.

I also would like to thank all those who have supported me and inspired me during my studies. Especially, I would like to thank my family for their support throughout my entire life. I love you with all my heart. Thank you for your encouraging words and your supports. Thank you for believing in me. I am grateful to my mom; her love kept me

strong even during the most difficult days and my dad for his unreserved support in my life. Finally, I wish to express my deepest thanks to my fiancée, *Nava*, for her patience and her continuing support during my study. I appreciate your understanding and being full of love and support; thank you for making my life so colourful.

Morteza Jeyhani
November 19, 2013

Contents

List of Figures

List of Tables

Nomenclature

V_{Max}	Maximum velocity (m/s)
$\acute{u}$	Fluctuation component in x-direction (m/s)
$\acute{v}$	Fluctuation component in y-direction (m/s)
$\overline{\rho \acute{u}\acute{u}}$	Reynolds normal stress in x-direction ([m/s]^2)
$\overline{\rho \acute{u}\acute{v}}$	Reynolds shear stress ([m/s]^2)
$\overline{\rho \acute{v}\acute{v}}$	Reynolds normal stress in y-direction ([m/s]^2)
ΔA	Interrogation area (mm^2)
μ	Dynamic viscosity (Kg/ms)
ε	Viscous dissipation of energy (Pa/s)
Δt	Time interval (s)
$MnGRAD$	Mean pressure gradient (mmHg)
N	Number of images
VTI	Velocity time integral (m)
du	Velocity difference in *x*-direction (m/s)
dv	Velocity difference in *y*-direction (m/s)

dx	Spatial resolution in x-direction (mm)
dy	Spatial resolution in y-direction (mm)
t	Time (s)
u	Velocity component in x-direction (m/s)
v	Velocity component in y-direction (m/s)
ρ	Density (kg/m^3)

Abbreviations

DO	Double-Orifice
DPIV	Digital Particle Image Velocimetry
EtER	Mitral Valve Repair Edge-to-Edge
GOA	Geometric Orifice Area
KE	Kinetic Energy
LA	Left Atrium
LV	Left Ventricle
MR	Mitral Regurgitation
MV	Mitral Valve
PEtER	Percutaneous Mitral Valve Repair Edge-to-Edge
PIV	Particle Image Velocimetry
RSS	Reynolds Shear Stress
TMPG	Transmitral Pressure Gradient

Chapter 1: Introduction

1.1 Overview

Our body needs oxygen to continue the process of life. Heart -a beating muscular pump about the size of your fist- connected to a network of arteries and veins pumps blood through the whole body. This complex system pumps at a rate of approximately 10 pints of blood per minute to both the body and the lungs.

The oxygen-rich blood from the aorta goes through the arteries and capillaries to convey blood to the different tissues, and disposes of waste products, like carbon dioxide. De-oxygenated blood returns to the right side of the heart through inferior and superior vena cavas. The right atrium ejects blood into the right ventricle through the tricuspid valve, and is then pumped through the pulmonary valve to the pulmonary artery. After passing through the lungs, blood goes to the left side of the heart through four pulmonary veins and reaches the left atrium (LA). Blood continues its journey into the left ventricle (LV) through the mitral valve (MV) and, finally, it is ejected into the aorta and the arterial system through the aortic valve.

Mitral valve and left ventricle filling phase (diastole)

The mitral valve is the main focus of this thesis. Its role is to ensure a strict, unidirectional movement of blood from the left atrium to the left ventricle. The left ventricular diastolic filling phase is characterized by a first jet emerging from the LA

through the MV, into the LV cavity as a result of ventricular expansion (E-wave), which is followed by a transitional phase (diastasis), and a second jet resulting from LA contraction (A-wave) (Nichols et al., 2011).

In this chapter, the MV anatomy, physiology and pathology are presented, followed by a discussion of the most common MV diseases and their proper repairs.

1.2 Mitral Valve Anatomy

The mitral valve comprises two leaflets, papillary muscles, chordae tendineae, the mitral annulus and the left ventricular myocardium (Figure 1.1). Imperfections in any of these components may result in blood flowing back into the left atrium during ventricular ejection.

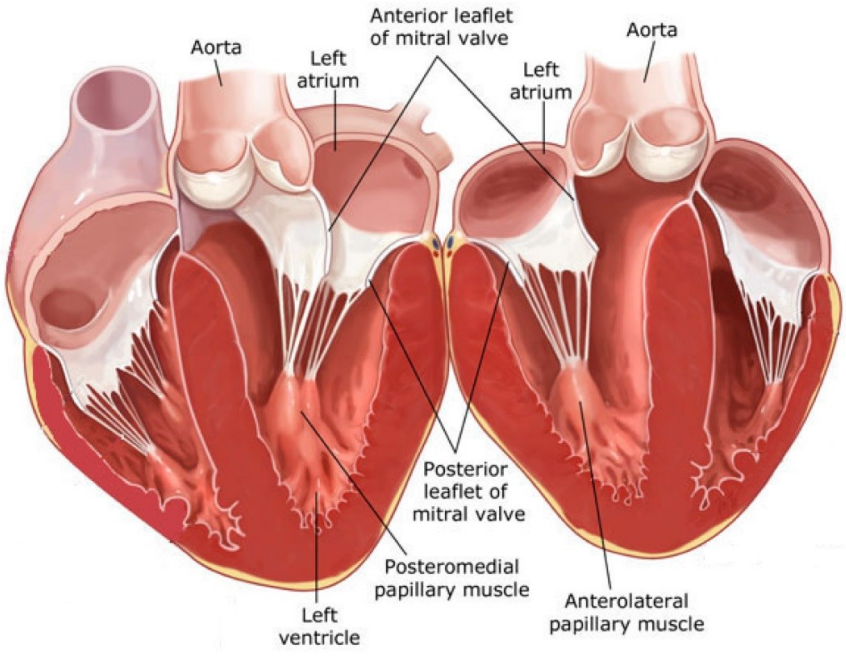

Figure 1-1: *An anatomic drawing of heart (https://www.themitralvalve.org)*.

1.2.1 Valvular Leaflets

The MV has two leaflets. The anterior leaflet has a semi-circular shape and the posterior leaflet has a quadrangular shape, which both are attached at their bases to the fibromuscular ring. The posterior leaflet is divided into three individual scallops with two indentations that are identified as P1, P2, and P3. The edge of the anterior leaflet is artificially divided into three portions, A1, A2, and A3 (Figure 1.2) (Lancellotti et al., 2010).

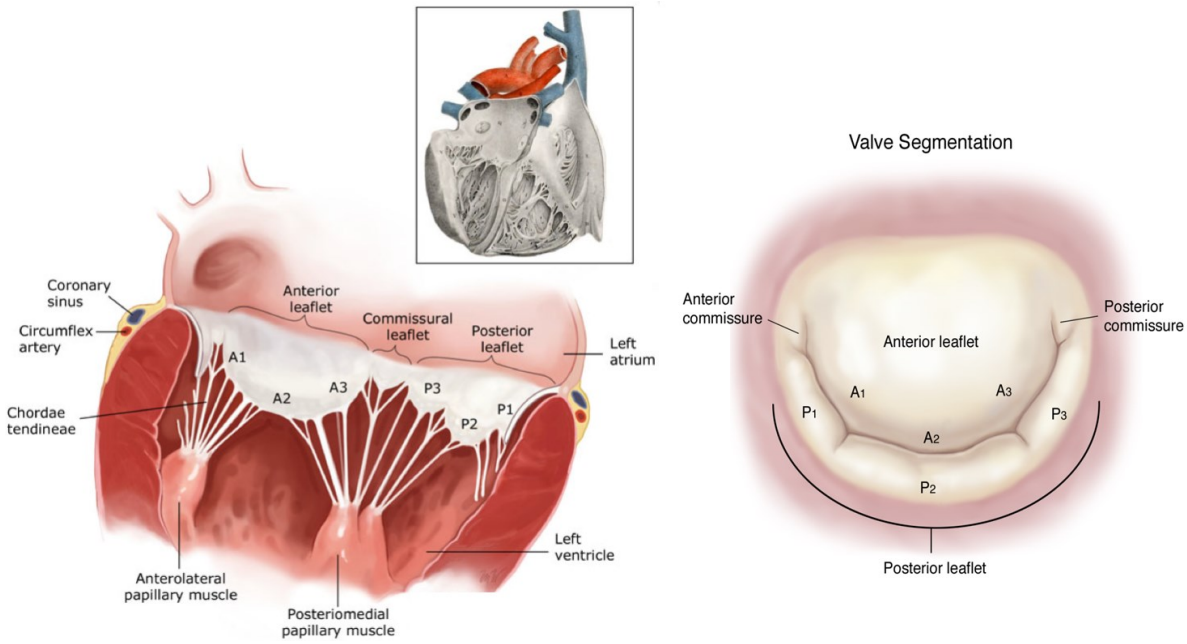

Figure 1-2: *Segmental anatomy of the mitral valve (https://www.themitralvalve.org).*

1.2.2 The Annulus

The mitral annulus constructs the anatomical junction between the left atrium and the left ventricle, and is the location of the insertion of the anterior and posterior leaflets. The

mitral annulus itself is divided into posterior and anterior segments. The anterior segment is attached to the fibrous trigons and the posterior segment is less developed. The mitral annulus has a saddle shape.

1.2.3 Subvalvular Apparatus

The subvalvular apparatus consists of chordae tendinae and papillary muscles. The chordae tendinae connect papillary muscles to the MV leaflets. The connection points are located between the free edge and the base of the leaflets. Rupture, calcification, fusion and redundancy of the chordae can cause mitral regurgitation. There are two papillary muscles arising from the apical area of the left ventricle. The anterolateral papillary muscle is mostly comprised of one head, or body, and the posteromedial papillary muscle may have two heads, or two bodies. Rupture, fibrotic elongation, or the displacement of papillary muscles may also lead to mitral valve regurgitation (Figure 1.3).

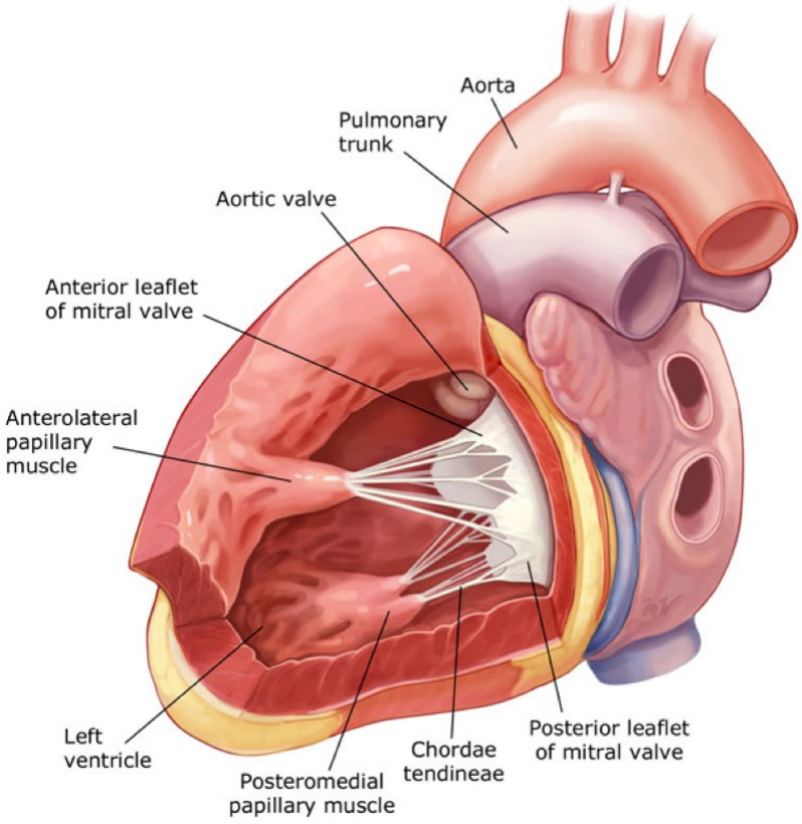

Figure 1-3: *Subvalvular apparatusin LV (https://www.themitralvalve.org).*

1.2.4 Left Ventricle (LV)

The papillary muscles are attached to the lateral wall of the LV, so any change in ventricular geometry may affect the mitral coaptation area. As a consequence, the LV is an important part of the MV complex (O'Gara et al., 2008).

1.3 Mitral Valve Pathology

Most cases of mitral valve defects are degenerative, although rare cases can be congenital, due to rheumatic fever, or resulting from ischemic heart disorder.

There are several different types of heart disease that can affect MV function. The following section describes the three most frequent pathologies.

1.3.1 Mitral Stenosis

Mitral valve stenosis is a narrowing of the mitral valve opening area. The leaflets are usually thicker, leading to abnormal LV filling during diastole, and an increase in LV work. Rheumatic fever is the most common cause of mitral stenosis.

1.3.2 Mitral Valve Prolapse

Mitral valve prolapse is a condition in which MV leaflets do not close tightly because the mitral valve leaflets are floppy (Figure 1.4). As a result, when LV contracts (systolic phase), one or more of the leaflets lose out into the LA and blood may flow back into the LA, leading to potentially significant regurgitation. In some cases, MV prolapse does not cause backflow and the leaflets may have proper closure (http://www.nhlbi.nih.gov/health/health-topics/topics/mvp/).

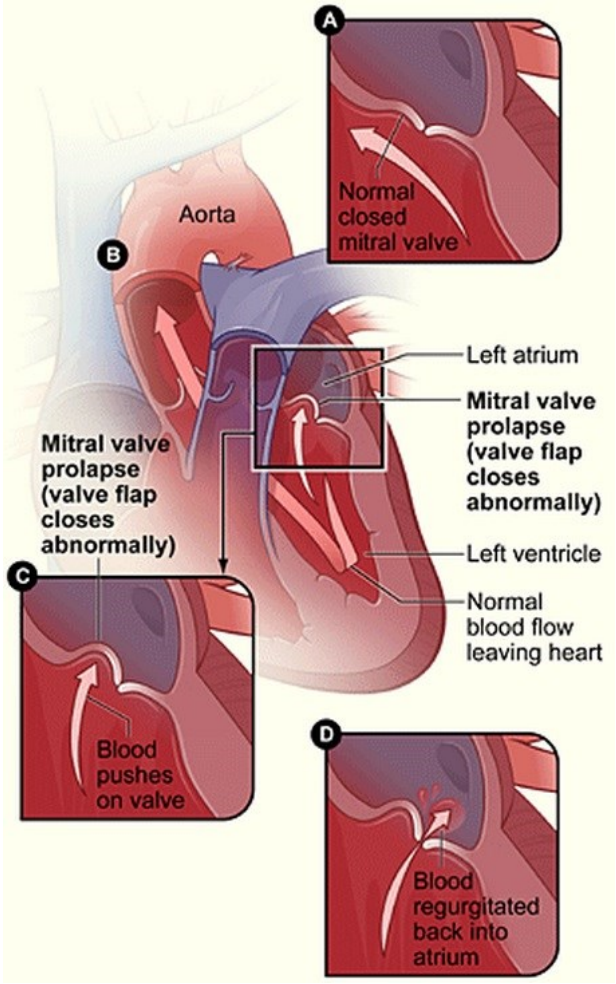

Figure 1-4: *Mitral valve prolapse (https: //www.nhlbi.nih.gov).*

1.3.3 Mitral Valve Regurgitation (MR)

Mitral regurgitation is a condition in which the mitral valve leaflets do not close securely during the systole (sometimes also called valvular insufficiency). This incomplete systolic closure leads to backflow to the LA. This pathological condition increases LV work, since, for each ejection phase, the LV has to compensate for the volume of blood flowing back into the LA, instead of through the aortic valve. MR can leads to LV dilatation, an increase in left atrium pressure, and pulmonary hypertension (Calafiore et

al., 2005). Approximately 500,000 people in North America alone are suffering from MR and each year.

There are two types of MR: acute and chronic. The acute type is characterized by pressure gradient in pulmonary veins which cause pulmonary edema. In chronic MR, the left atrial size increases slowly, so there is no pressure gradient in the pulmonary veins. Progressive ventricular dilation leads to dysfunction of the ventricle and, eventually, heart failure.

1.4 Mitral Valve Repair

Surgical valve repair is the best solution for symptomatic patients with severe MR (Bakker et al. 2013). Several reports have shown the superiority of MV repairs over MV replacements, including better preservation of LV function, lower thrombus formation, and increased survival rates (Gillinov et al., 2008). Approximately 50,000 mitral valve repairs are performed in the United States. (Rogers et al. 2011; Dang et al. 2005).

Several techniques can be used to repair a MV: Annuloplasty, quadrangular resection, re-suspension of leaflets, and edge-to-edge repair.

1.4.1 Annuloplasty

In this method, a cloth-covered ring is inserted around the mitral valve in order to ensure optimal coaptation of the valve leaflets, and to minimize regurgitation. Severe undersized annuloplasty can, however, lead to mitral stenosis (Figure 1.5).

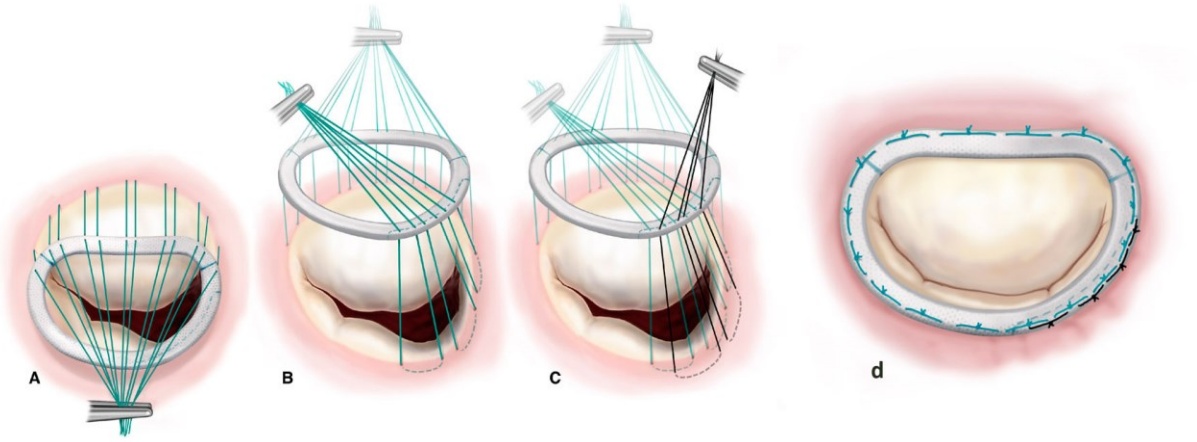

Figure 1-5: *Mitral valve annuluplasty (https://www.themitralvalve.org).*

1.4.2 Quadrangular Resection

One of the problems seen in mitral regurgitation is prolapse of the middle portion of the posterior leaflet (P2) that it may results from the rupture of chordae tendineae. In such case quadrangular resection is a method in which the loose, redundant segments of the leaflets are removed (Figure 1.6. I).

1.4.3 Re-Suspension of Leaflets

In cases with elongated or broken chords valve's leaflet needs artificial chordae tendineae to prevent prolapsing; also sometimes additional chords are required to support loosen leaflets. This procedure named re-suspension of leaflets with artificial chords (Figure 1.6. II).

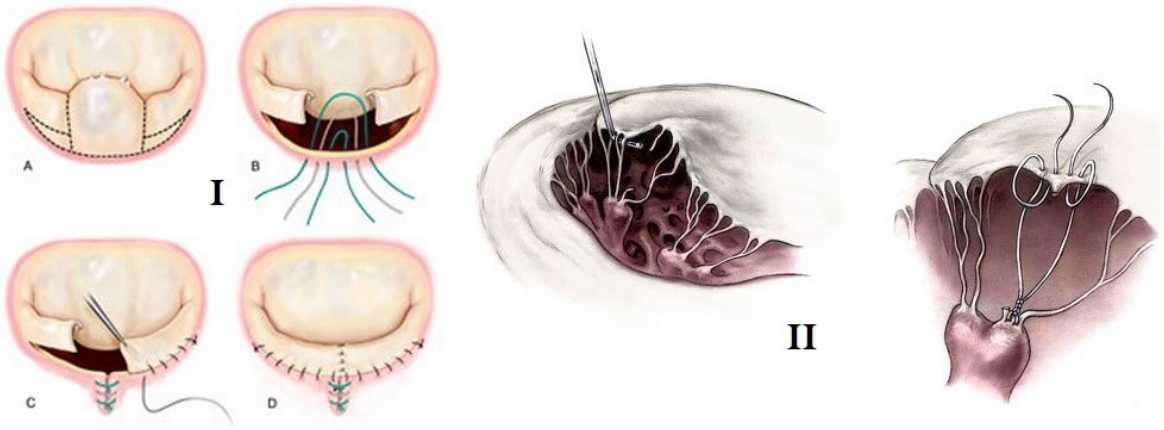

Figure 1-6: *I: Mitral valve quadrangular resection (https://www.themitralvalve.org); II: Artificial chordae (https://www. ctsnet.org).*

1.4.4 Percutaneous Edge-to-Edge Repair

Although the above mentioned approaches to surgical repair have already been applied successfully, recent European reports show that as many as 49% of patients with MR are denied surgery because they are considered to be “high risk” patients, due to comorbidities, LV dysfunction, or age (Jamieson et al., 1999; Vahanian et al., 2007; Mirabel et al., 2007; Estevez-Louriero et al., 2013). For these patients, the most recent guidelines set by the European Society of Cardiology suggest considering percutaneous Edge-to-Edge mitral valve Repair (PEtER). EtER consists of locally suturing together the diseased free edges of the posterior and anterior MV leaflets exactly where the regurgitant jet is located (Fucci et al., 1987). Percutaneous EtER originates from the surgical approach developed by Alfieri et al. (2001). Application of the EtER for cases with regurgitant jets in the center of the MV leads to a double orifice (DO) valve configuration. For the cases in which MV lesion is localized near to the commissure, surgical technique of edge-to-edge repair results in a single orifice with a rather smaller

area that is named paracommissural repair (Alfieri et al., 2005); (Figure 1.7). The proper implementation of this technique in treating valve regurgitation has led to low risk, and good early and mid-term clinical results and can be used as a standardized procedure (Maisano et al., 2000).

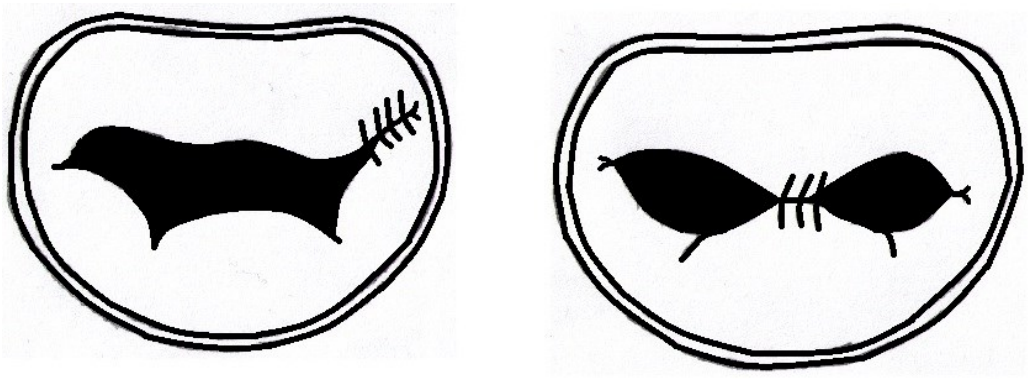

Figure 1-7: *The percutaneous EtER technique. Right: Double orifice (DO). Left: Paracommissural repair*.

This procedure can be minimally invasive by using a clip (MitraClip©). The MitraClip (Abbot Vascular, Santa Clara, California, USA) approach is an option to treat MR with determined clinical success (Rogers et al., 2011). The MitraClip device mimicks the EtER technique. The device is composed of a cobalt chromium implant with two arms and two grippers that are used to snatch the edges of the two leaflets in order to improve leaflet coaptation and results in a double orifice valve configuration (Rogers et al., 2013); (Figure 1.8).

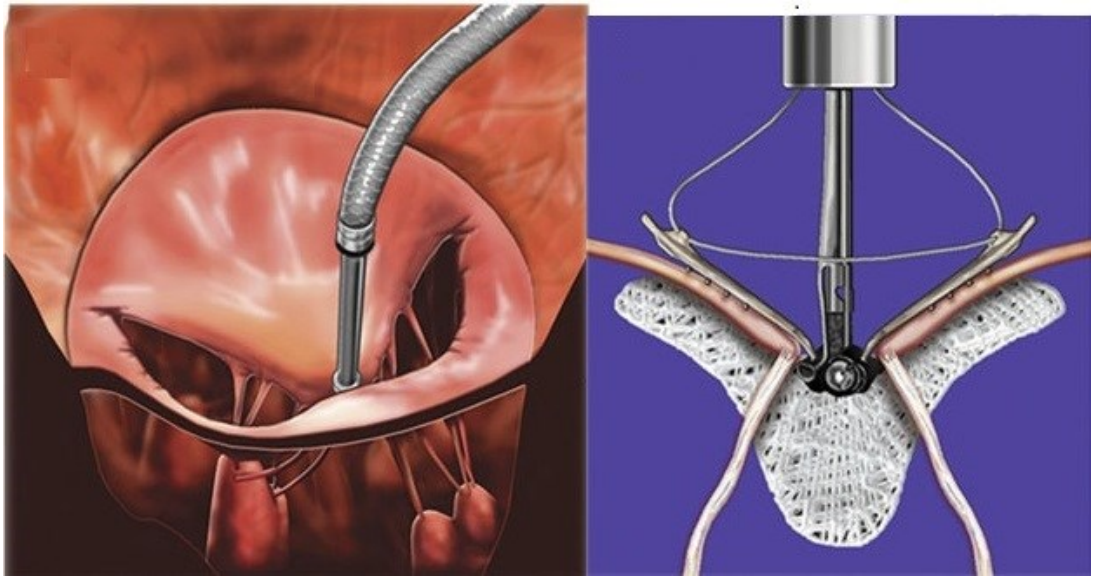

Figure 1-8: *Schematic of MitraClip (Rogers et al., 2013).*

Successful clip placement can be achieved in the majority of patients (typically above 95%) (Van den Branden et al., 2012). Under such valve opening configurations, the assessment of MV hemodynamics is challenging and little is known regarding induced flow patterns in the LV (Loh et al., 2013).

1.5 Literature Review

1.5.1 Flow in Left Ventricle with a Healthy Mitral Valve

Pedrizzetti et al. (2005) numerically evaluated the optimization of the swirling flow in the human LV under physiological conditions. They showed that the location of the mitral valve is optimal in order to ensure the smooth continuity between cardiac phases (diastole and systole) and to minimize energy dissipation.

Schiller et al. (2006) tried to simulate blood flow in the left part of the human heart to see the changes in flow patterns and energy loss. They used a virtual heart model, which was created based on a real human heart. By the aim of MRI got time-depending geometry and intraventricular flow from healthy human LV and left atrium. They performed the numerical flow calculation with a finite volume method. Experiments that consist of a silicon ventricle with the exact geometry of the virtual ventricle with the PIV and LDA measurement were used for validation. Combination of MRI –flow measurements and numerical simulation data show the effect of procedural influences. Furthermore, the numerical study provides them with the opportunity to perform intraventricular energy estimations.

Hong et al. (2008) tried to evaluate the possibility of analyzing the left ventricular vortex by using contrast echocardiography and determining the LV vortex flow in MR cases, as well as with patients with LV systolic dysfunction. This study included twenty-five patients that underwent contrast to evaluate vortices and velocity vectors. In this study, they quantified LV vorticity with the aid of contrast echocardiography in normal and dysfunctional LV during systole.

1.5.2 Flow in Left Ventricle with Mitral Valve Repaired Using Edge-to-Edge Technique

Percutaneous EtER originates from the surgical approach developed by Alfieri et al. (2001). It is currently performed using a MitraClip (Abbot Vascular, Santa Clara,

California, USA), and involves clipping the free edges of the valve leaflets at the non-coaptation zone of the regurgitant jet (Hilberath et al., 2013).

Edge-to-edge repair of the mitral is expected to significantly modify the flow patterns in the LV and leads to a double-orifice MV opening. Successful clip placement can be achieved for most patients (typically above 95%) (Van den Branden et al., 2012). Under such valve opening configuration, the assessment of MV hemodynamics is challenging and little is known regarding induced flow patterns in the LV (Loh et al., 2013). Maisano's group have performed interesting numerical simulations on surgical edge-to-edge approach. The results were very informative, and demonstrated that the velocity profile downstream of the double-orifice MV is similar to a healthy, single-orifice valve with the same geometrical orifice area (Maisano et al., 1999). Furthermore, they showed that the generated "camel-like" velocity profile can lead to up to 35% variation in the estimation of mitral transvalvular pressure gradient depending on the location of the measurements. Such flow patterns have also been confirmed by Hu et al. (2010), through 3D numerical simulations, using finite volume method, of the flow in the LV following edge-to-edge repair. They also showed that the double orifice configuration creates two strong jets with the maximum of 1.05 m/s and small-scale vortices that are rapidly convected towards LV apex. Moreover, they showed that the flow in the LV, following edge-to-edge repair, induces elevated viscous energy losses. They also showed that percutaneous edge-to-edge repair might contribute to a reduction in LV filling efficiency.

From a physiological point of view, the abnormal flow pattern in the LV, following edge-to-edge repair, lead to elevated shear regions in the LV. This can trigger the thromboembolic process. Interestingly, Orban et al. (2012) reported the case of a patient with successful percutaneous edge-to-edge MV repair who developed a large left ventricular thrombus four days after the repair.

1.5.3 Summary of Literature Review

This literature review has shown that:

- The flow in a normal left ventricle is optimized in order to allow for a smooth continuity between filling and ejections phase with minimal energy loss.
- Edge-to-edge mitral valve repair significantly alters flow patterns in the left ventricle, reduces its filling efficiency, and can potentially lead to thrombus formation.
- Only few numerical studies have investigated flow patterns in the left ventricle following edge-to-edge mitral valve repair. There are, so far, no *in vivo*, or experimental works.

1.6 Objectives

The main objective of this thesis is to investigate experimental flow patterns in the left ventricle following simulated edge-to-edge repair. The hemodyanmics of the mitral valve will be evaluated using standard clinical approaches and the flow patterns will be measured using particle image velocimetry.

Chapter 2 : *In vitro* Experimental Setup and Conditions

2.1 Experimental Facility

2.1.1 ViVitro System

For the purpose of this study, a ViVitro pulse duplicator (ViVitro Labs, Victoria, BC, Canada) was used (Figure 2.1). This system is capable of reproducing normal human physiological conditions in terms of pressure and flow waveforms.

Figure 2-1: *ViVitro pulse duplicator (ViVitro Labs, Victoria, BC, Canada).*

This system is powered by a piston-in-cylinder pulsatile pump. The setup includes an atrium chamber that contains a mitral valve, a silicone model of the left ventricle, and a rigid glass model of the ascending aorta. The arterial system consists of a compliance chamber and a resistance. Flow through the MV was measured using an electromagnetic flow meter (Carolina Medical Electronics, King, NC, USA) with 10% accuracy on the full-scale (5 ml/min to 20 l/min). Pressure measurements were performed using Millar MPC 500 transducers (Millar Instruments, Houston, TX, USA), with an accuracy of +- 0.025% on the full scale (-50 mmHg to 300 mmHg).

Figure 2.2 sketches the close-loop circulation circuit. It comprises the resistive element (simulating peripheral body resistance) and a compliance chamber (simulating the elasticity of the arteries).

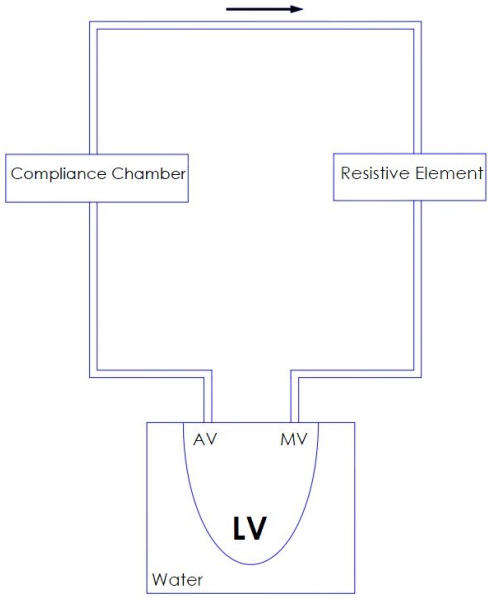

Figure 2-2: *Scheme of close-loop circulatory system.*

This chapter also discusses the different components of the left heart simulator.

2.1.2 Valves Configurations

One of the most challenging parts of this project was developing the model of a mitral valve. The system includes a trileaflet bioprosthetic valve in the mitral position. The shape of the model valve is far from the shape of an anatomical mitral valve. However, developing an anatomically realistic mitral valve would require adding models of the papillary muscles and the chordae to the model, limiting the flow visualization by particle image velocimetry. To overcome this, two approaches have been considered; 1) developing rigid models of mitral valves, before and after edge-to-edge repair, and; 2) developing a custom-made mitral valve and an original solution to avoid leaflet prolapse.

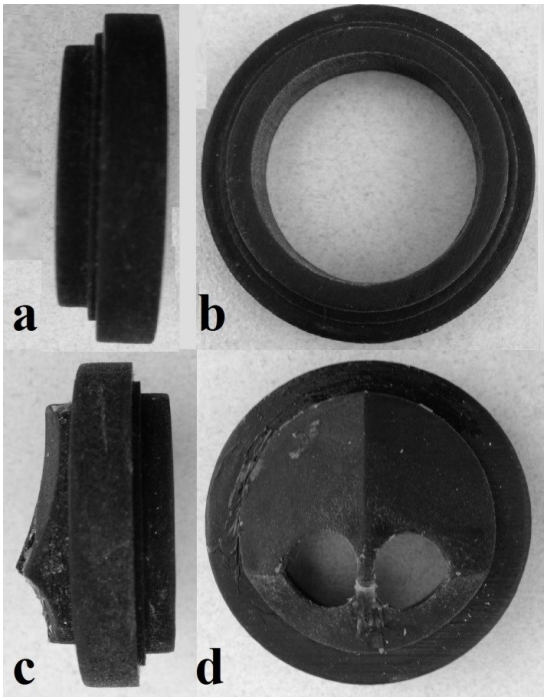

Figure 2-3: *a) Side view b) Top view of healthy valve configuration. c) Side view d) top view of percutaneous edge-to-edge repaired mitral valve configuration.*

Several measurements have been done on the rigid model. The results were very informative but the lack of consideration of the dynamic movement of the leaflets was a significant limitation. For the custom-made mitral valve, several designs have been tested. A mitral valve annulus has been designed and rapid-prototyped. For the valve leaflets, in terms of material properties, the silicon-made leaflets were first tested. However, their durability during the testing was not satisfactory, as the leaflets eventually tore. New leaflets made from rubber bands directly cut from a balloon, were then tested. The durability of the rubber valves was significantly better compared to the silicon valves. The problem of leaflet prolapses was solved using a new approach. Four thin wires (diameter of 0.3 mm) were positioned at the level of the mitral annulus. As a consequence, during left ventricle ejection, the wires prevented the valve leaflets from flipping back into the left atrium. It was verified that the size of the wires was small enough to avoid significant disturbance in the flow. Indeed, the computed Reynolds number (based on peak E-wave velocity and wire diameter) for the flow around the wires was 142 and, under such conditions, a steady separation bubble should exist downstream of the wires.

On this custom-made mitral valve, two configurations have been tested; 1) a regurgitant valve, and; 2) a repaired valve using percutaneous edge-to-edge technique. A 4 mm width patch at the middle portion of the leaflets simulated the latest configuration. The width of the patch was selected to mimic the cobalt-chromium clip used in transcatheter edge-to-edge MV repair using the MitraClip system (Abbott Vascular, Santa Clara, California).

The geometrical orifice area of the valve before percutaneous EtER was 572 mm^2, while the total geometrical orifice area of the generated double-orifice was 245 mm^2.

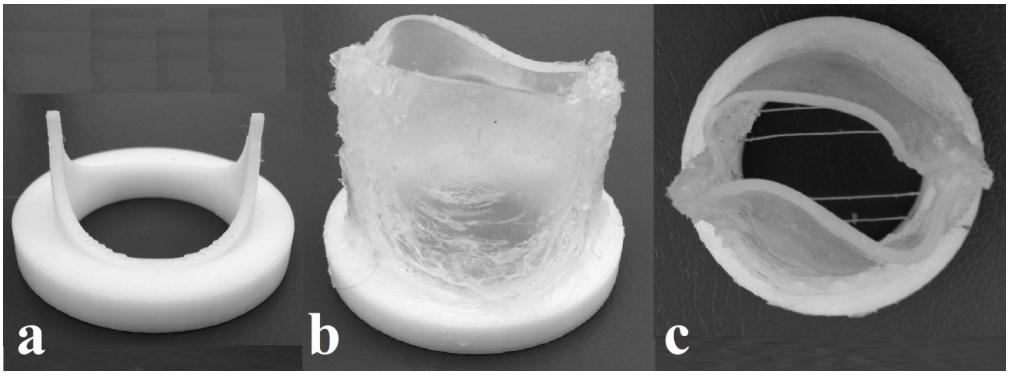

Figure 2-4: *a) Annulus base b) Mitral valve configuration with silicon leaflets. c) Four wires at the level of annulus.*

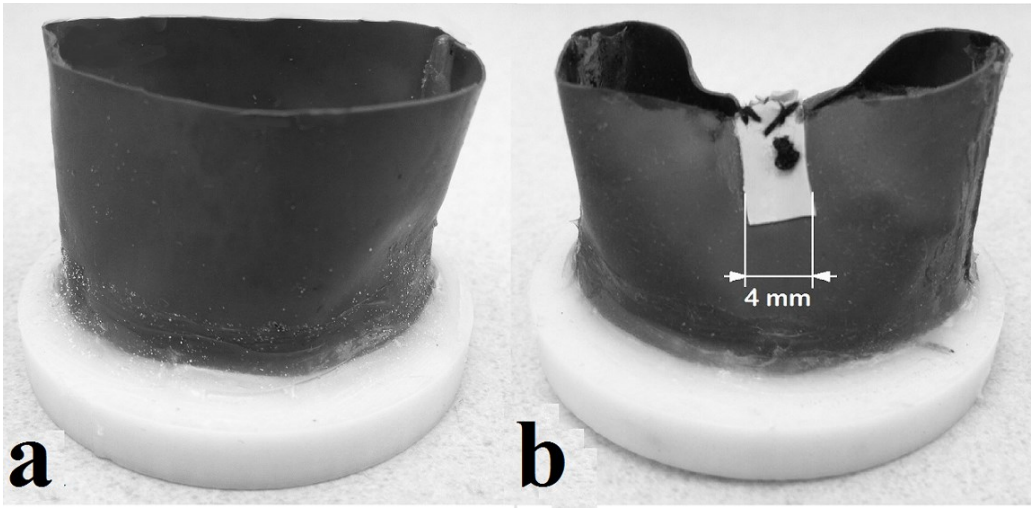

Figure 2-5: *a) Mitral valve in MR condition b) Mitral valve after percutaneous EtER.*

2.1.3 Particle Image Velocimetry

Particle Image Velocimetry, or PIV, is an optical technique allowing instantaneous velocity measurements on a whole plane (Raffel et al., 2006). A standard PIV system requires a laser source, CCD Camera(s) and light scattering particles.

The principle of PIV is quite straightforward; the laser emits light that is scattered by the particles. Two consecutive images of the particles, with a determined time delay Δt, are recorded by a high-speed camera. The images are then divided into interrogations zones (typically 32 by 32 pixels, or less) and cross-correlation is then performed between the two images. The peak of the cross-correlation in each interrogation region leads to the most probable displacement of the particles within specific zone. Knowing the time delay Δt between the images, the local velocity can easily be determined (Figure 2.6).

In this work, PIV has been used in order to investigate the velocity field inside the LV for both valve configurations (MR and EtER).

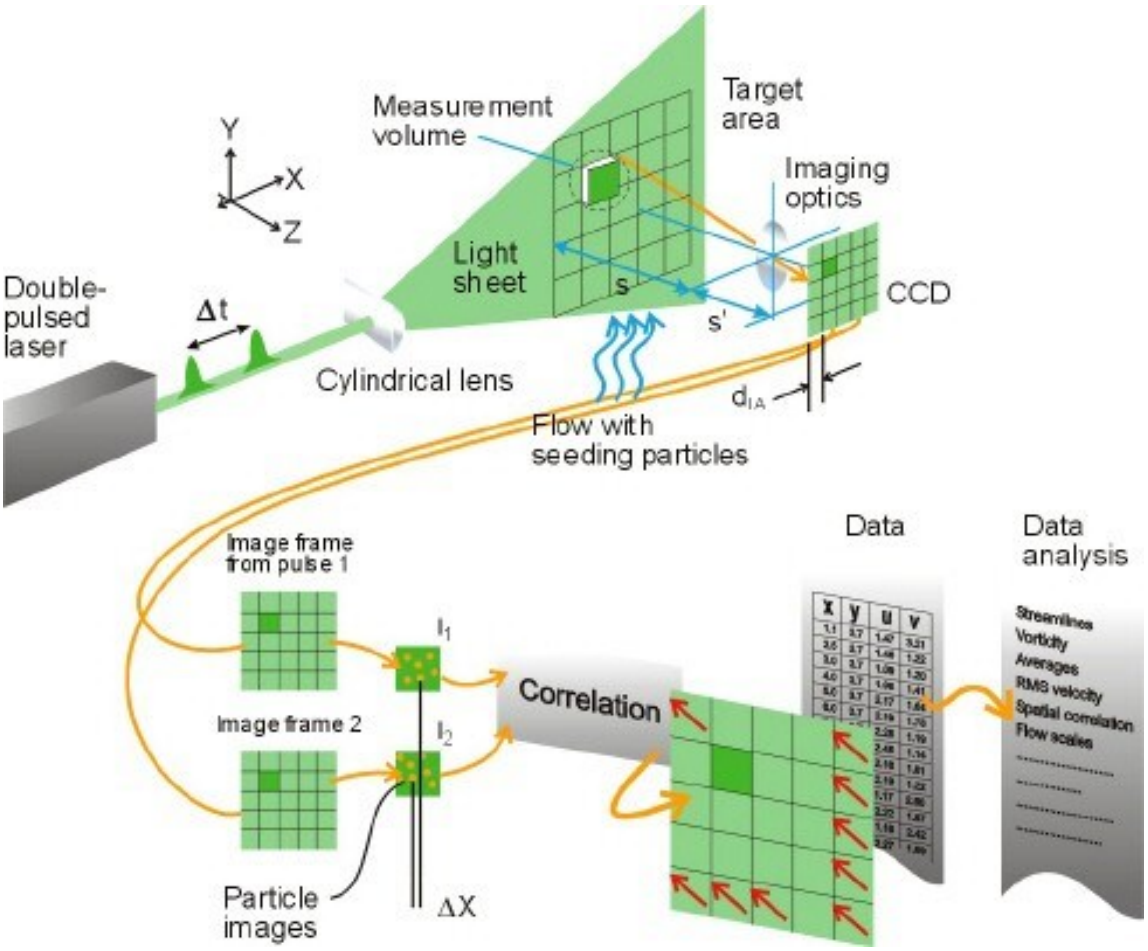

Figure 2-6: *PIV setup (Dantecdynamics.com).*

2.1.3.1 Laser

The PIV LaVision system (LaVision GmbH, Goettingen, Germany) was used in combination with a dual cavity Nd:YLF laser (Litron Lasers, Warwickshire, UK) with a maximum pulse energy of 10 mJ at 527 nm and a maximum repetition rate of 20 kHz. The laser sheet, with a thickness of approximately 1 mm; was positioned parallel to the MV flow jet (Figure 2.7).

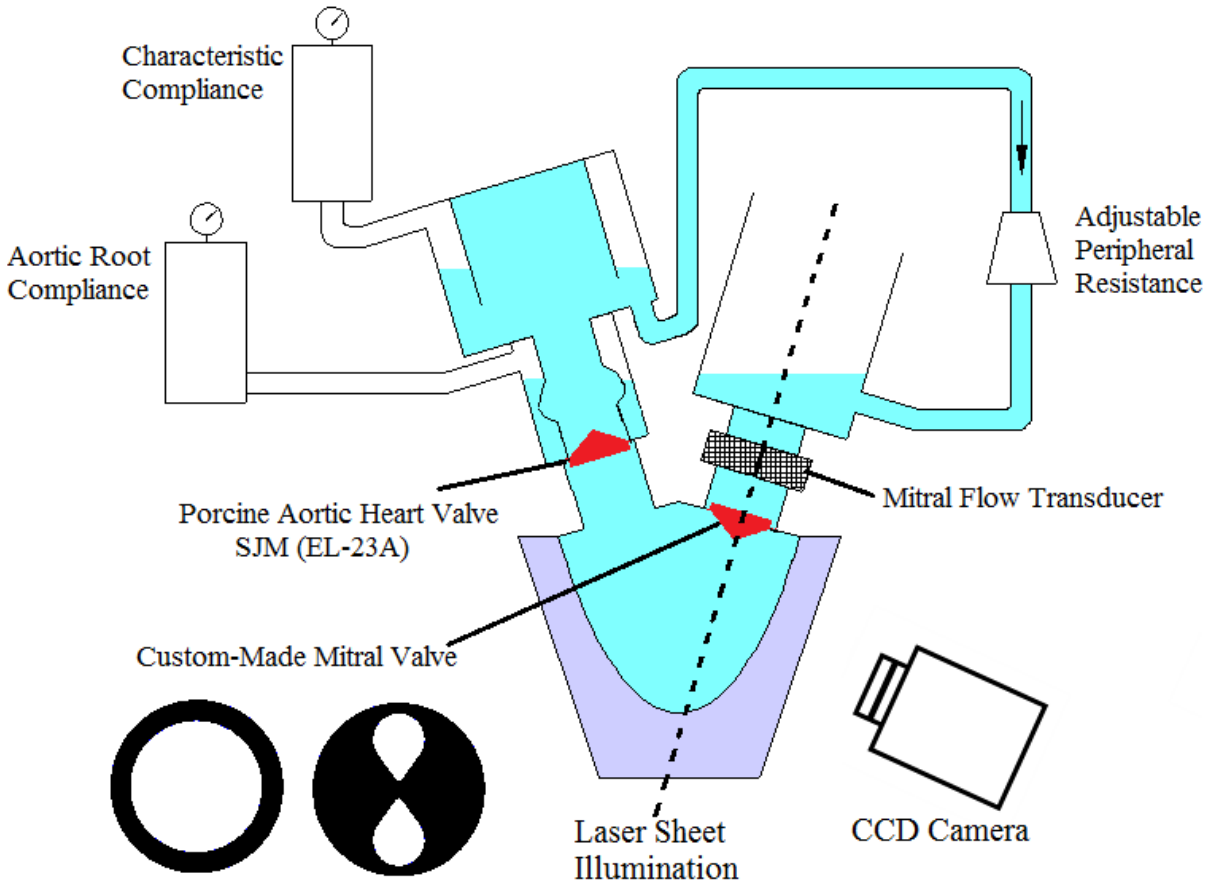

Figure 2-7:*Schematic of the ViVitro System cardiac simulator addressing the position of laser sheet illumination and position of CCD camera.*

2.1.3.2 Seeding Particles

The seeding particles are an important and critical part of PIV system because the particles must match the fluid properties. The particles must be small enough to be able to follow the fluid flow (reduction of Stokes drag), but at the same time, large enough to scatter enough light. Another important characteristic required from the seeding particles for cardiovascular flow applications is their time response. The particles have to be

capable of rapidly responding to sudden variations in flow velocity. In this work, Hollow Glass Spheres of 10 μm diameters and a density of 1.1 g/cm³ were found to adequately respond to the above mentioned constraints.

2.1.3.3 Camera

A high-speed digital camera (Phantom V9.1, Vision Research, NJ, USA) with 1000 fps, at a maximal resolution of 1632×1200 pixels was used for recording the images. The maximal recording frequency achievable at full resolution is then 500 Hz. In order to optimize the cross-correlation of the PIV measurements for each instant of measurement, the time step between two consecutive laser pulses (Δt) was modified to satisfy the ¼ law (Δt range: 100 μs to 700 μs) (Raffel et al., 2006). Both phase-locked and time-resolved measurements have been performed. For phase-locked measurements, a total of 200 images was recorded for each phase, and was then averaged. Multi-pass cross-correlations were used with an initial interrogation region size of 32×32 pixels, and a final size of 16×16 pixels, with 50% overlapping. The final spatial resolution was 0.49 mm × 0.49 mm.

2.1.4 Doppler Echocardiography

In order to compare the results found in this work with *in vivo* data that is available in the literature, Doppler echocardiographic measurements have been performed. Doppler echocardiography measurements were performed using an Acuson 128 XP/10

(California, USA) and V219 (2.5 MHz) probe (Figure 2.8). The beam was carefully aligned with the main jet direction. For the double-orifice configuration, the beam was aligned with one of the orifices. For all measurements, continuous-wave Doppler was used and the following parameters were determined: 1) Peak E-wave velocity; 2) Peak and mean transvalvular pressure gradient using simplified Bernoulli equation (Eq. 2.1).

$$\Delta P = 4V^2 \qquad (Eq. 2.1)$$

That V stands for the velocity downstream of the mitral and ΔP for the transmitral pressure gradient.

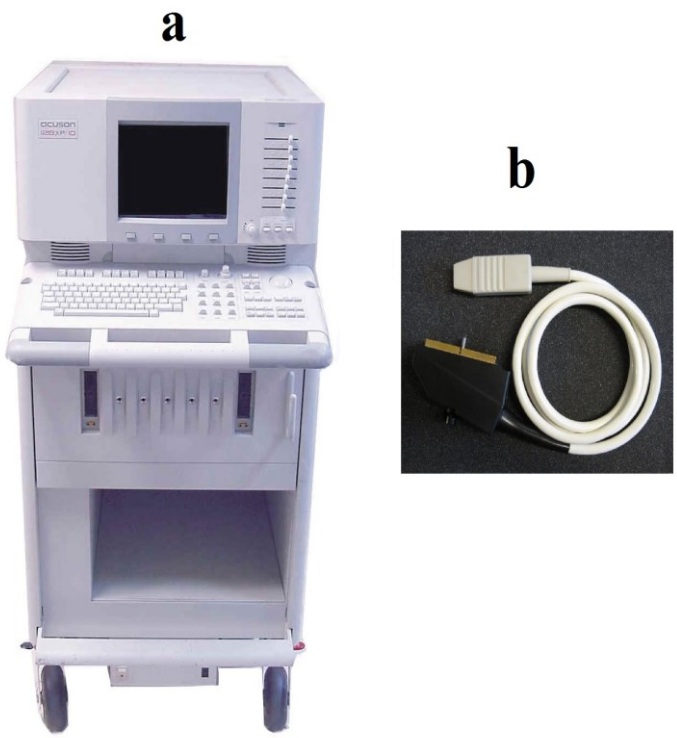

Figure 2-8: *a) Doppler echocardiography measurements were performed using an Acuson 128 XP/10 (California, USA) with b) V219 (2.5 MHz) probe that plugged* to the *Doppler echocardiography to perform the measurements.*

2.1.5 Catheter Measurements

Pressure waveforms in left heart cavities were recorded using three standard Millar catheters MPR-500 with the accuracy of ±0.025% on the full scale (-50 ml/min to 20 l/min). Additionally, pressure measurements were performed upstream and downstream of the mitral valve using a new pressure wire developed by HemoDynamix Inc. Based on fiber-optic technology, the prototype designed by HemoDynamix Medical Systems incorporates 4 sensors, spaced 2 cm apart, within an envelope of 0.71 mm of outside diameter. This diameter is small enough for the device to be guided to heart valve regions within a standard guiding catheter (which has an inner diameter of 0.89 mm or 0.035"). Apertures were created on the envelope using a laser so that the pressure sensors have access to the surrounding environment. Radio-opaque marker bands indicate the location of pressure sensors. The device is terminated with a flexible "J-tip" to reduce the possibility of damage to heart tissues (Figure 2.9).

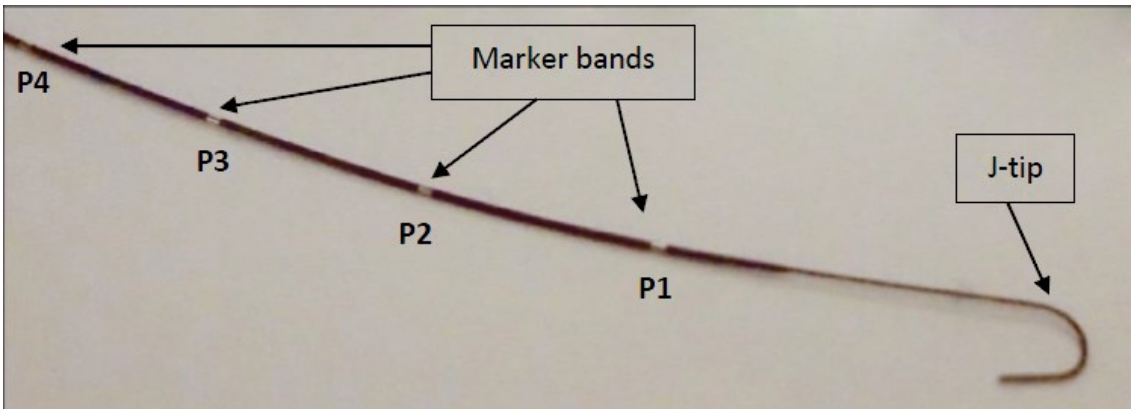

Figure 2-9: *Multisensory device for endovascular with four sensors and flexible J-tip.*

Figure 2-10: *The evolution chassis unit.*

The device was connected to a FISO (evolution Chassis) designed computer-controlled signal conditioner and data acquisition to be able to read pressures (Figure 2.10). On the prototype used in the study, only two sensors were functional. One sensor was located upstream of the MV model, and a second one at the tip of the valve leaflets. For the double-orifice case, the probe was passed through one of the orifices.

Mitral flow waveform was measured using an electromagnetic Carolina Medical Electronics flow probe. The internal diameter of the probe is defined at 28 mm, and matches the aortic and MV flow channels in the system. A FM501 flow meter was used with the flow probe.

2.2 Experimental Conditions

The measurements were performed under physiological conditions: heart rate of 70 bpm, arterial systolic and diastolic pressures of 120 mmHg and 80 mmHg, stroke volume of 70 mL. The circulatory fluid was a mixture of water and glycerol with a density of 1080

kg/m^3 and viscosity of 3.5 cP to simulate the physiological characteristics of the blood under high shear rate conditions.

Phase-Locked PIV measurements were performed at 8 different instants during diastole (See Figure 2.11).

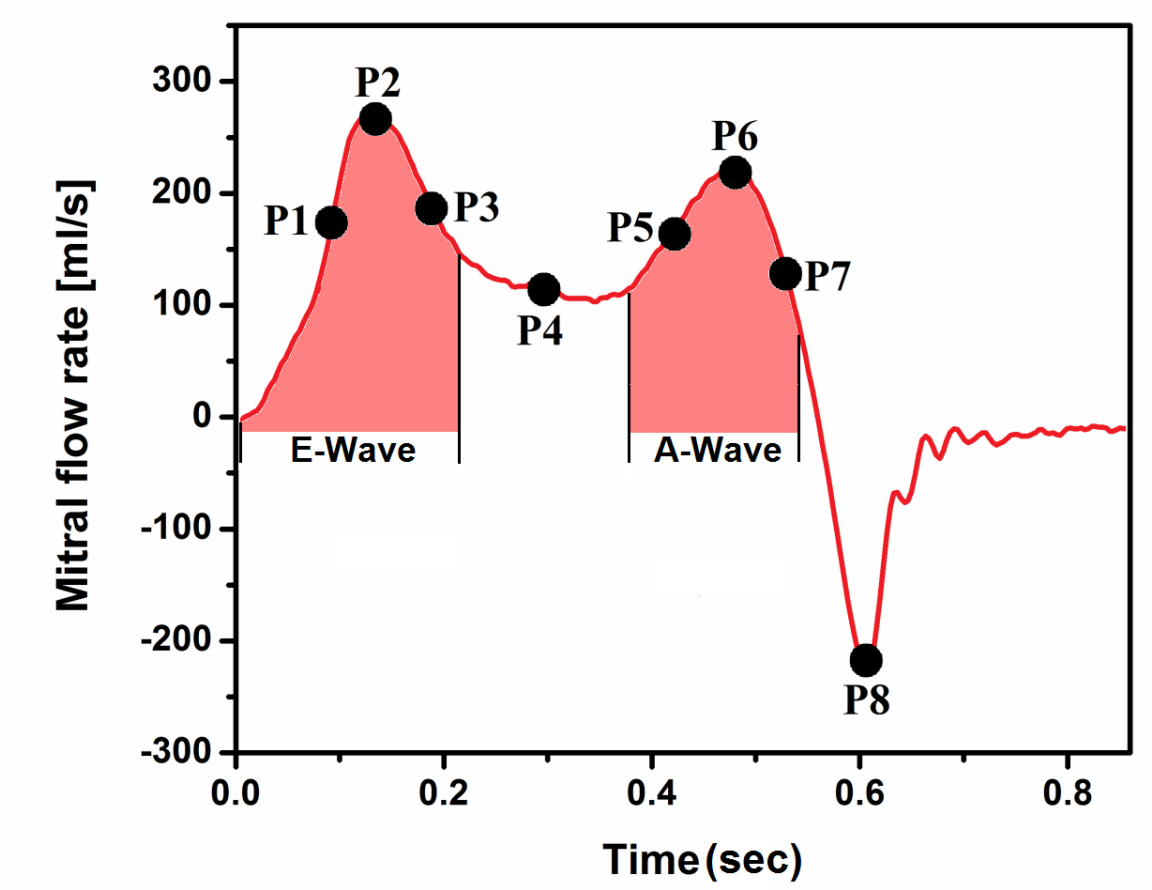

Figure 2-11: *PIV measurements performed in seven points during diastole and one point in systole.*

Chapter 3 : Results

In this section, the experimental results obtained with the two configurations of the mitral valve, the regurgitant mitral valve and the mitral valve following edge-to-edge repair, are presented and discussed.

3.1 Mitral Flow Waveform

Figures 3.1 and 3.2 show flow waveform through the mitral valve before and after percutaneous edge-to-edge repair. It is worth noting that simulated EtER successfully reduced mitral valve regurgitant volume (integral of the flow rate moving back from the left ventricle to the atrium during systole) from 34 ml to 15 ml (56% reduction). So, in this work, a severe mitral regurgitation was simulated and the edge-to-edge repair approach led to a reduction in its severity to mild mitral regurgitation. This is consistent with *in vivo* findings were several studies have shown that percutaneous edge-to-edge repair successfully reduced mitral regurgitation from grade 4 (severe mitral regurgitation) to grade 3 or 2 (moderate or mild mitral regurgitation) (Bakker et al., 2013; Van den Branden et al., 2007). It is important to note that only in a limited number of cases, percutaneous edge-to-edge repair led to more than two-grade reduction in mitral regurgitation.

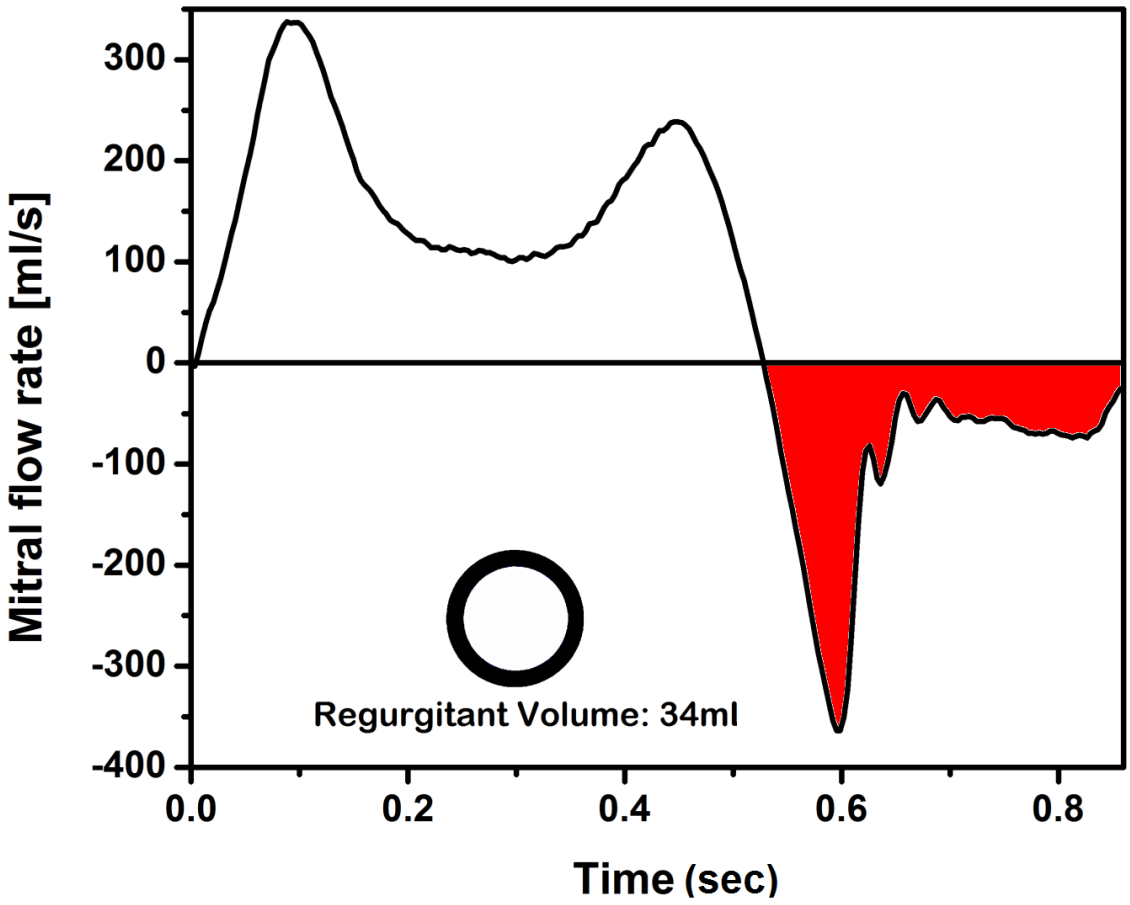

Figure 3-1: *Mitral flow waveform before simulated percutaneous EtER. Red color zone shows that the regurgitant volume is 34 ml.*

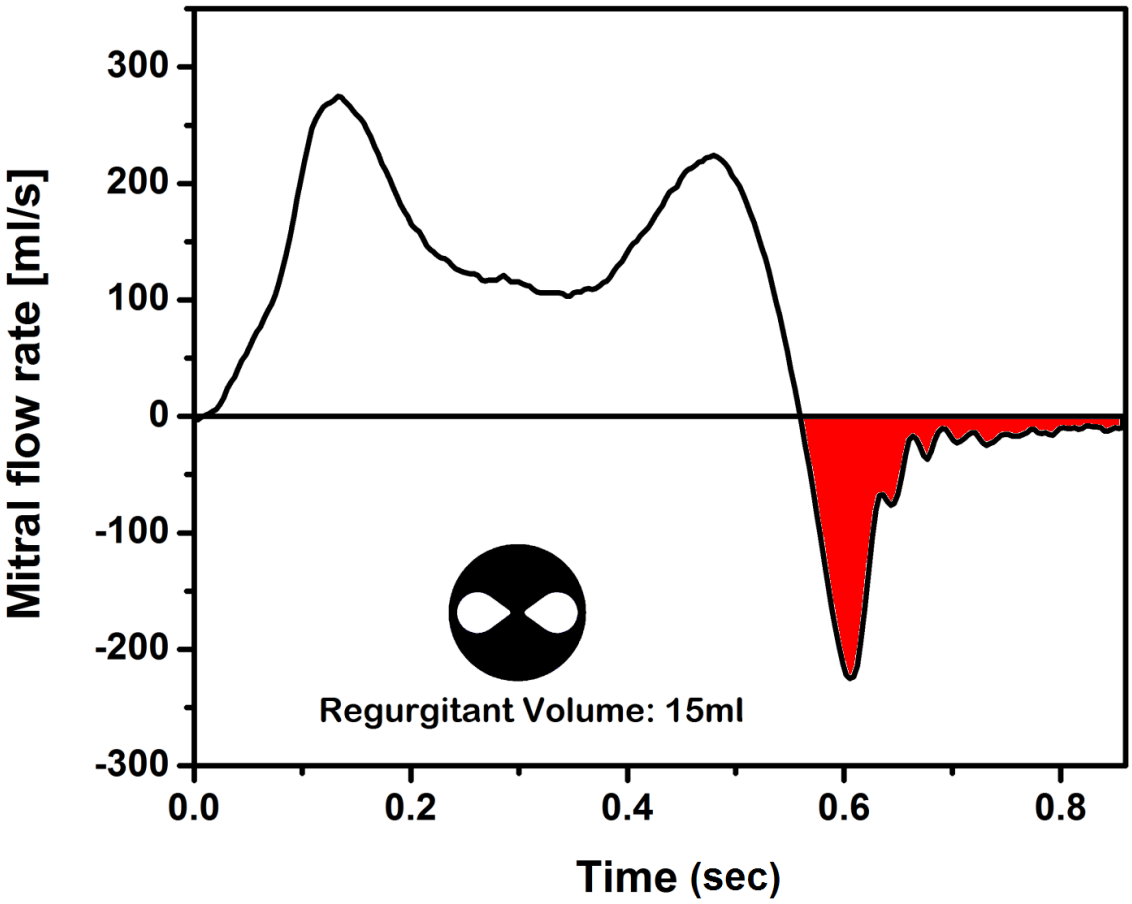

Figure 3-2: *Mitral flow waveform before simulated percutaneous EtER. Red color zone shows that the regurgitant volume to 15 ml.*

3.2 Doppler Echocardiography and Catheter Measurements

A major concern with percutaneous edge-to-edge repair is the possibility of inducing a significant flow restriction through the mitral valve during LV systole. Indeed, the significant reduction in the mitral valve geometrical orifice area following edge-to-edge repair might lead to a mitral stenosis. However, clinical evaluations of mitral valve

performance following percutaneous edge-to-edge repair is challenging due to the double orifice configuration of the valve. In this work, unique experiment measurements using both Doppler echocardiography and catheterization allow a direct comparison between the pressure losses induced by the mitral valve during systole, following edge-to-edge repair.

The beam of Doppler was aligned with one of the orifices and, for all the measurements performed, continuous-wave Doppler was used and the following parameters were determined: velocity-time integral (VTI); mean transmitral pressure gradient (MnGRAD); peak E-wave velocity and peak A-wave velocity. The table 3.1 shows the obtained data:

Table 3-1: *Continues-wave Doppler for PEtER.*

VTI (m)	***MnGRAD (mmHg)***	***E-Wave (m/s)***	***A-Wave (m/s)***
0.54	*4.6*	*1.65*	*1.30*
0.54	*4.6*	*1.58*	*1.28*
0.50	*4.3*	*1.65*	*1.28*

$$TMPG = 4V_{max}^2 \qquad (Eq. 3.1)$$

For catheter measurements, one sensor was located upstream of the MV model, and a second one at the level of the tip of the value leaflets. The probe was passed through one

of the orifices for the double-orifice case. The comparison between Doppler echocardiography and catheter measurements is shown in the figure 3.3:

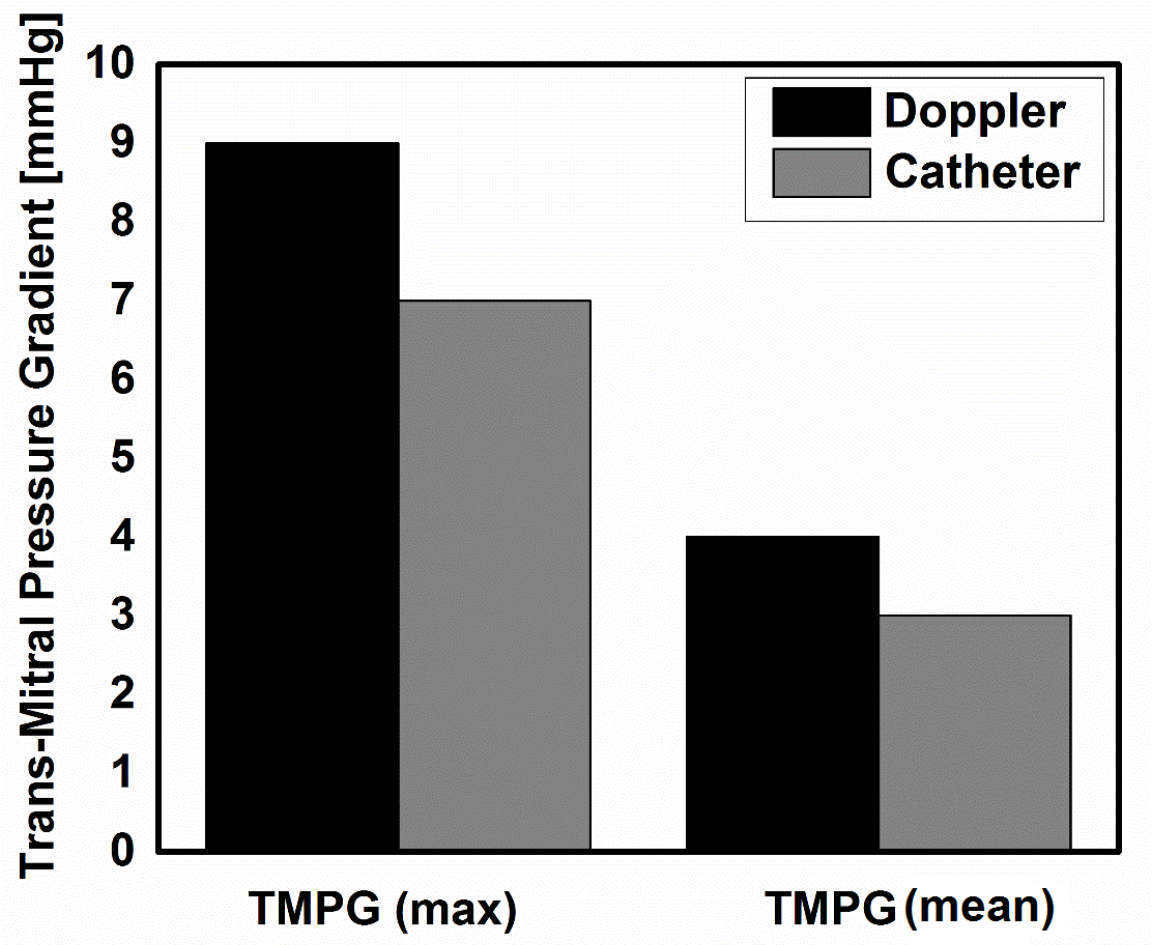

Figure 3-3: *Comparison between Doppler and catheter transmitral pressure gradients. There is a good agreement between the two measurements and the EtER seems not to induce a severe mitral stenosis.*

The figure displays peak and mean transmitral pressure gradients (TMPG), as measured by catheter and Doppler ultrasounds. There was good agreement between the results. The peak of TMPG for the Doppler is 9 mmHg, which is close to the peak of TMPG

measured by catheter (7 mmHg). The mean TMPG by the Doppler is 4 mmHg while it was 3 mmHg by catheter.

3.3 PIV Measurement

3.3.1 Phase-Locked Measurement

PIV measurements were taken at eight different instants (phases) during the cardiac cycle. Here, the three most important instants are discussed: peak of E-wave; mid-diastasis; and peak of A-wave.

3.3.1.1 Velocity Pattern and Profiles

Figure 3.4 shows the flow pattern inside the LV at the peak of E-wave. The simulated percutaneous edge-to-edge repair induced a clear modification in the flow inside the left ventricle. A double jet develops with a significant increase in maximal velocity from 0.4 m/s to 1.6 m/s.

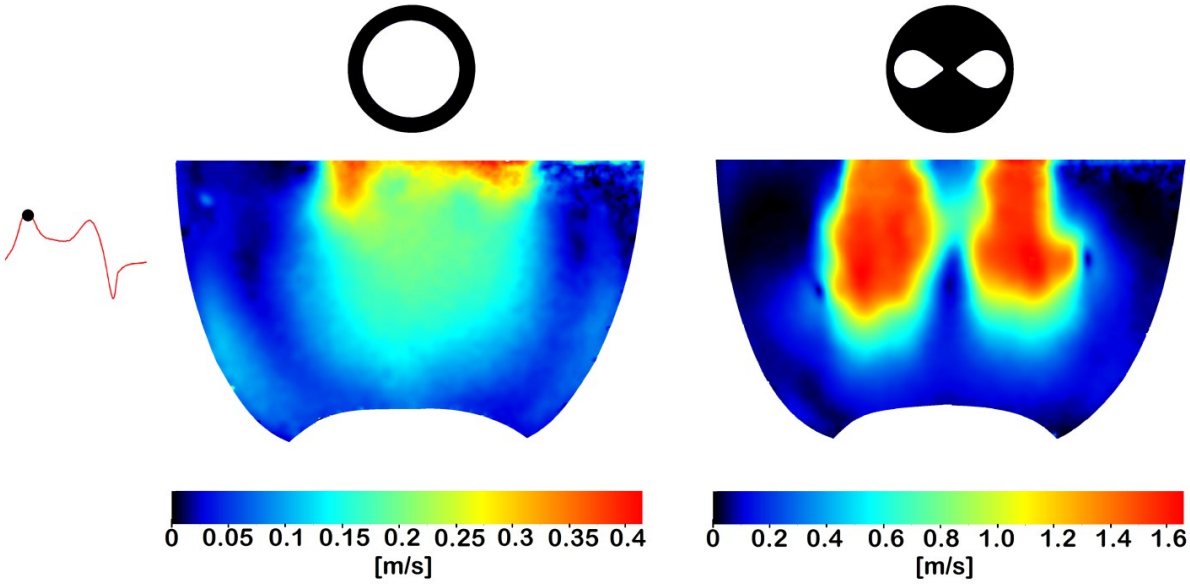

Figure 3-4: *Velocity patterns measured by particle image velocimetry at peak of E-wave. The measurements were performed before (left) and after (right) simulated percutaneous edge-to-edge mitral repair. The induced double jet configuration clearly appears with a deeper penetration inside the LV.*

Figure 3.5 shows the comparison of the velocity profile measured 15 mm downstream of the tip of the MV leaflets and at the peak of the E-wave. A clear difference between the case of regurgitant mitral valve and following percutaneous edge-to-edge repair can be observed. A 'double flat' velocity profile is generated following percutaneous edge-to-edge repair. Such velocity profiles increases shear layer zones and might predispose to shear induced blood components damage.

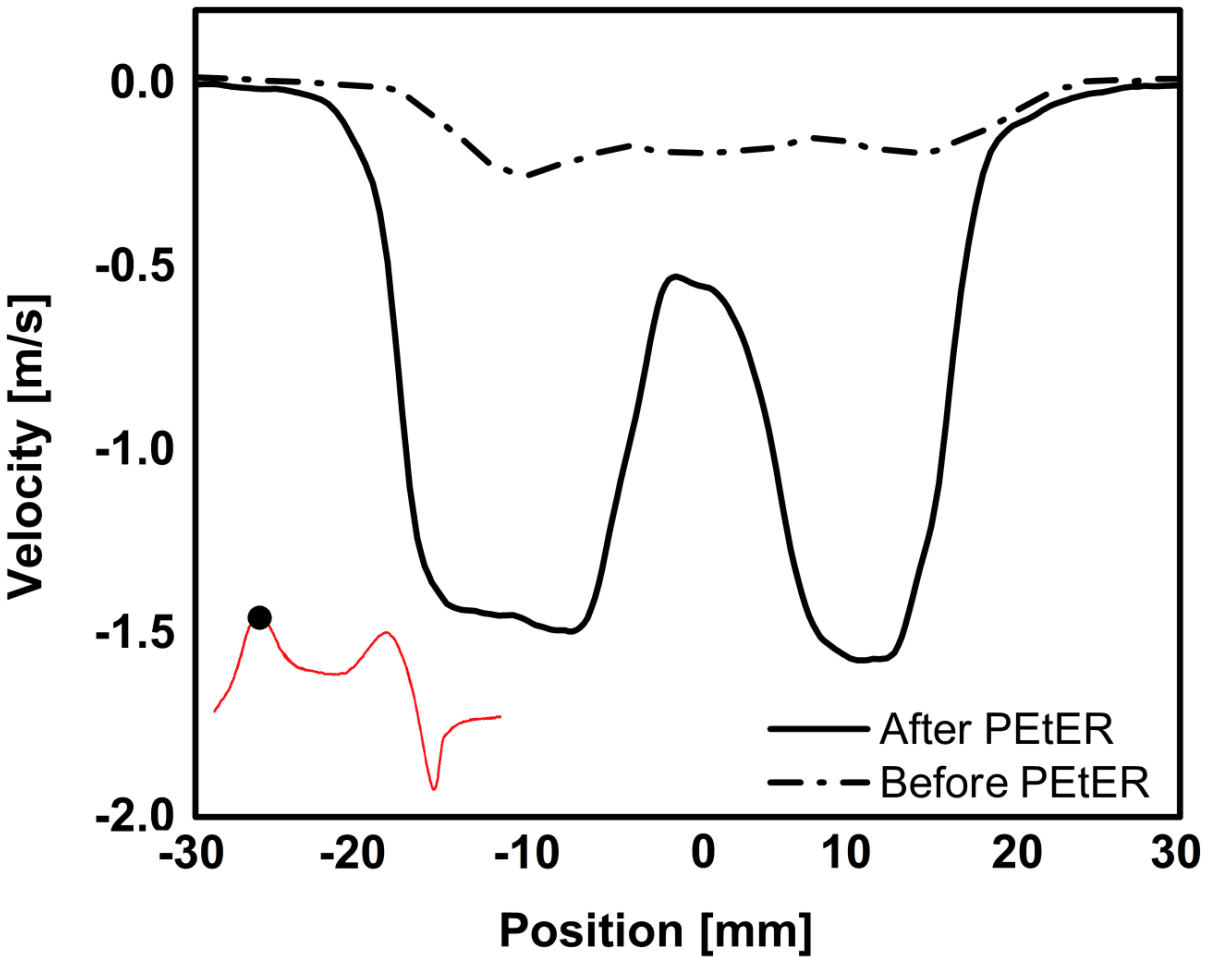

Figure 3-5: *Velocity profile measured by particle image velocimetry 15 mm downstream of the tip of the mitral valve leaflets for the peak of E-wave. The measurement was performed before and after percutaneous edge-to-edge mitral repair. The induced double jet configuration significantly increases the magnitude of the velocity and generates a double jet configuration.*

Figure 3.6 represents flow patterns inside the LV during diastasis. The reduction in mitral inflow leads to a reduction in maximal jet velocity compared to peak E-wave: 0.25 m/s for regurgitant mitral valve and 0.8 m/s following percutaneous edge-to-edge repair. The

velocity profiles measured 15 mm downstream of the tip of the mitral valve leaflets remain unchanged with a reduced velocity magnitude (Figure 3.7).

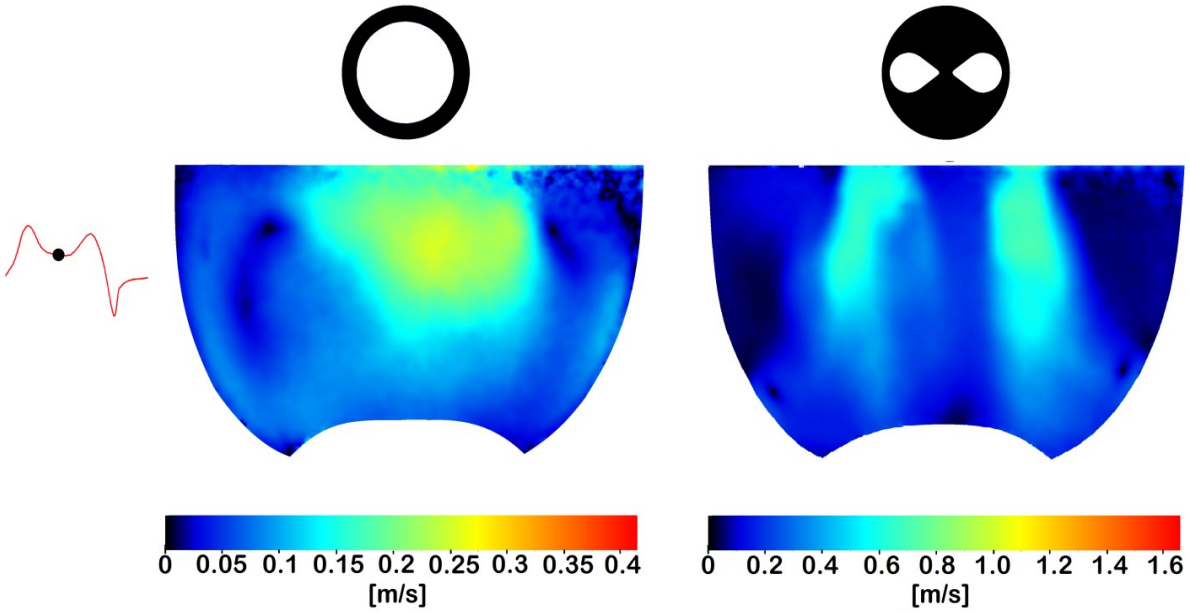

Figure 3-6: *Velocity patterns measured by particle image velocimetry at diastasis. The measurements were performed before (left) and after (right) simulated percutaneous edge-to-edge mitral repair. The induced double jet configuration clearly appears with a deeper penetration inside the LV.*

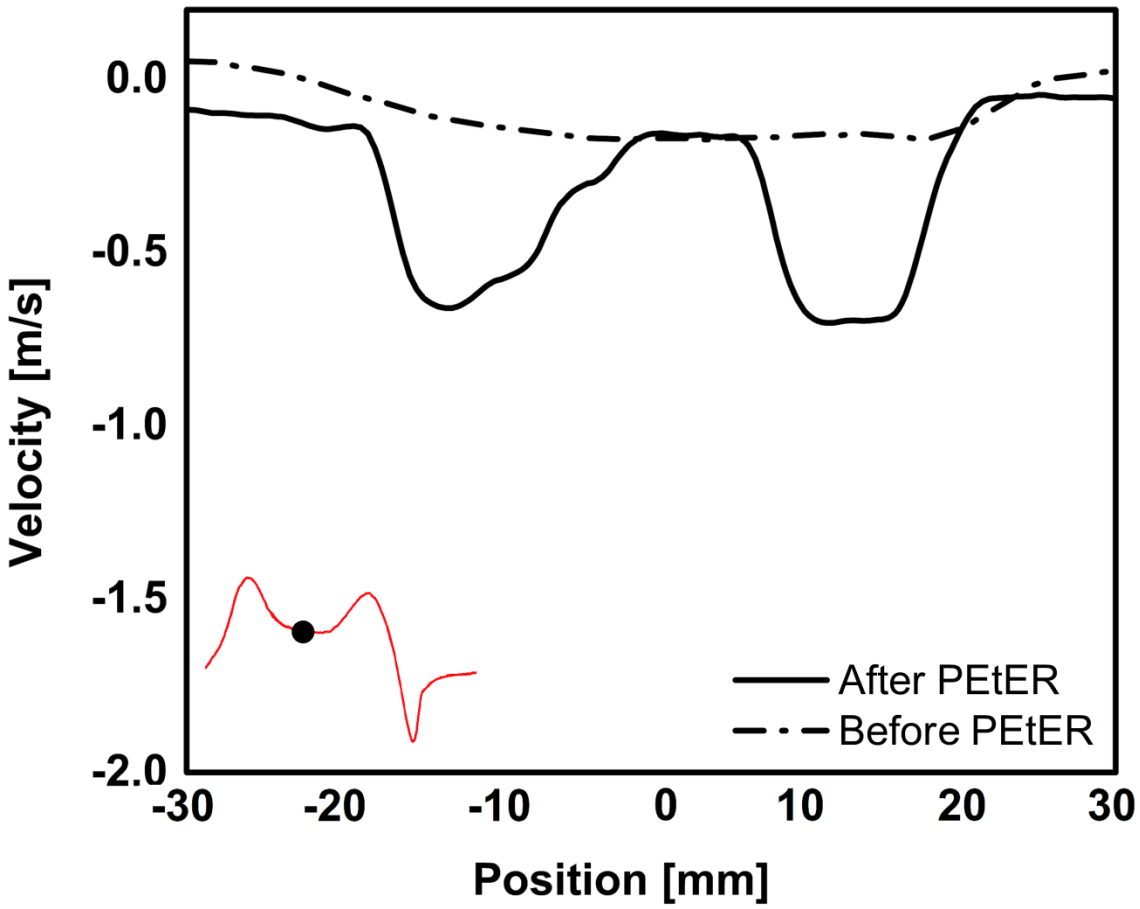

Figure 3-7: *Velocity profile measured by particle image velocimetry 15 mm downstream of the tip of the mitral valve leaflets for the diastasis. The measurement was performed before and after percutaneous edge-to-edge mitral repair. The induced double jet configuration significantly increases the magnitude of the velocity and generates a double jet configuration.*

The velocity magnitude at the peak of A-wave of flow rate through the mitral valve increases as a result of left atrium contraction. As a result, the velocity magnitude in the LV increases again to reach 0.3 m/s for mitral regurgitation case and 1.4 m/s following edge-to-edge repair (Figures 3.8 and 3.9).

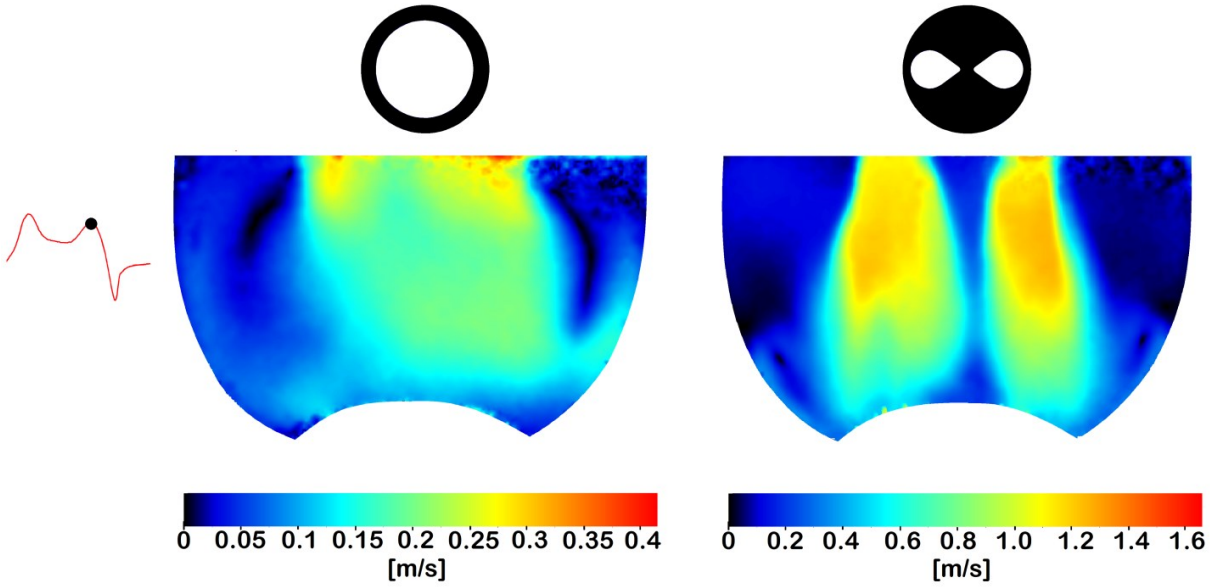

Figure 3-8: *Velocity patterns measured by particle image velocimetry at peak of A-wave. The measurements were performed before (left) and after (right) simulated percutaneous edge-to-edge mitral repair. The induced double jet configuration clearly appears with a deeper penetration inside the LV.*

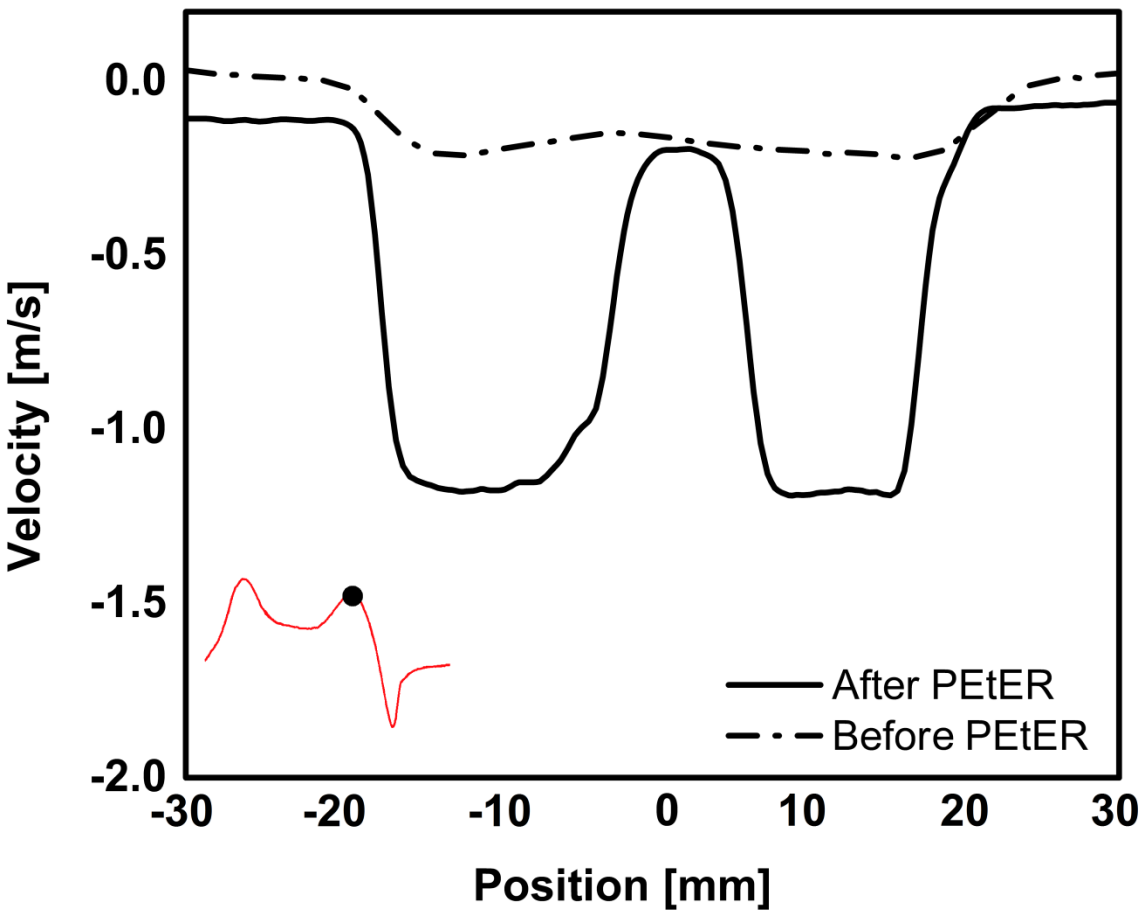

Figure 3-9: *Velocity profile measured by particle image velocimetry 15 mm downstream of the tip of the mitral valve leaflets for the A-Wave. The measurement was performed before and after percutaneous edge-to-edge mitral repair. The induced double jet configuration significantly increases the magnitude of the velocity and generates a double jet configuration.*

3.3.1.2 Streamlines

Plotting velocity streamlines allows for a better representation of flow structures in the left ventricle before and after percutaneous edge-to-edge repairs.

Figure 3.10 represents velocity streamlines at the peak of E-wave, diastasis, and peak of A-wave. In the case of mitral regurgitation, a large coherent structure develops in the left ventricle (a cross section of vortex ring). This structure is convected towards the left ventricle apex, and occupies a large portion of the ventricle cross-section at the end of diastole. Such a large coherent structure has been shown to play an important role in storing energy during diastole (Pedrizzetti et al., 2005). For the case following percutaneous edge-to-edge repair, a smaller coherent structure is developed in the left ventricle and is rapidly convected towards the apex. No large-scale coherent structure is present in the left ventricle prior to the ejection phase. This abnormal flow configuration might contribute to a sub-optimal ventricular performance (Hu et al., 2010).

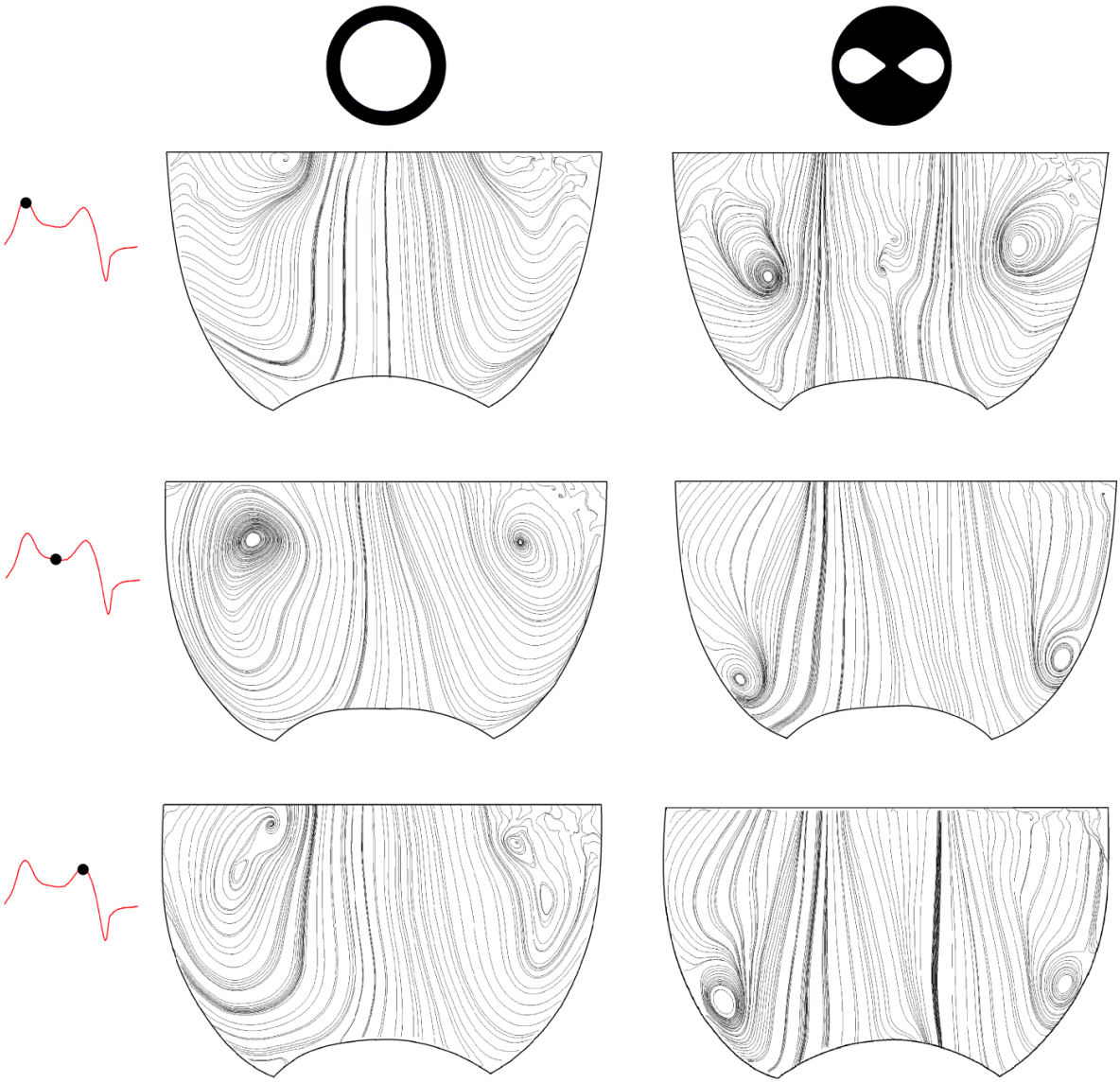

Figure 3-10: *Velocity streamlines measured by particle image velocimetry at three different instants. The measurements were performed before (left) and after (right) simulated percutaneous edge-to-edge mitral repair. EtER induced significant modifications in vortex development in the LV. following EtER the vortices were small, and rapidly convected to the LV.*

3.3.1.3 Total Kinetic Energy and Viscous Dissipation of Energy

A way to evaluate the performance of the left ventricle is to compute the total kinetic energy and the viscous dissipation of energy.

For kinetic energy per unit of mass at each phase (i), is computed as:

$$KE = \sum_i \frac{1}{2}\rho V_i^2 = \frac{1}{2}\rho \sum_i (u^2 + v^2)_i \Delta A \qquad (Eq. 3.1)$$

where ρ is the density of the fluid, u is the velocity component in x-direction, v is the velocity component in y-direction, and ΔA is the interrogation area in PIV. All local kinetic energies at each spatial location are added to represent the total kinetic energy at a specific instant in the cycle.

Figure 3.11 shows a map of the spatial distribution of kinetic energy at the peak E, and A wave of LV.

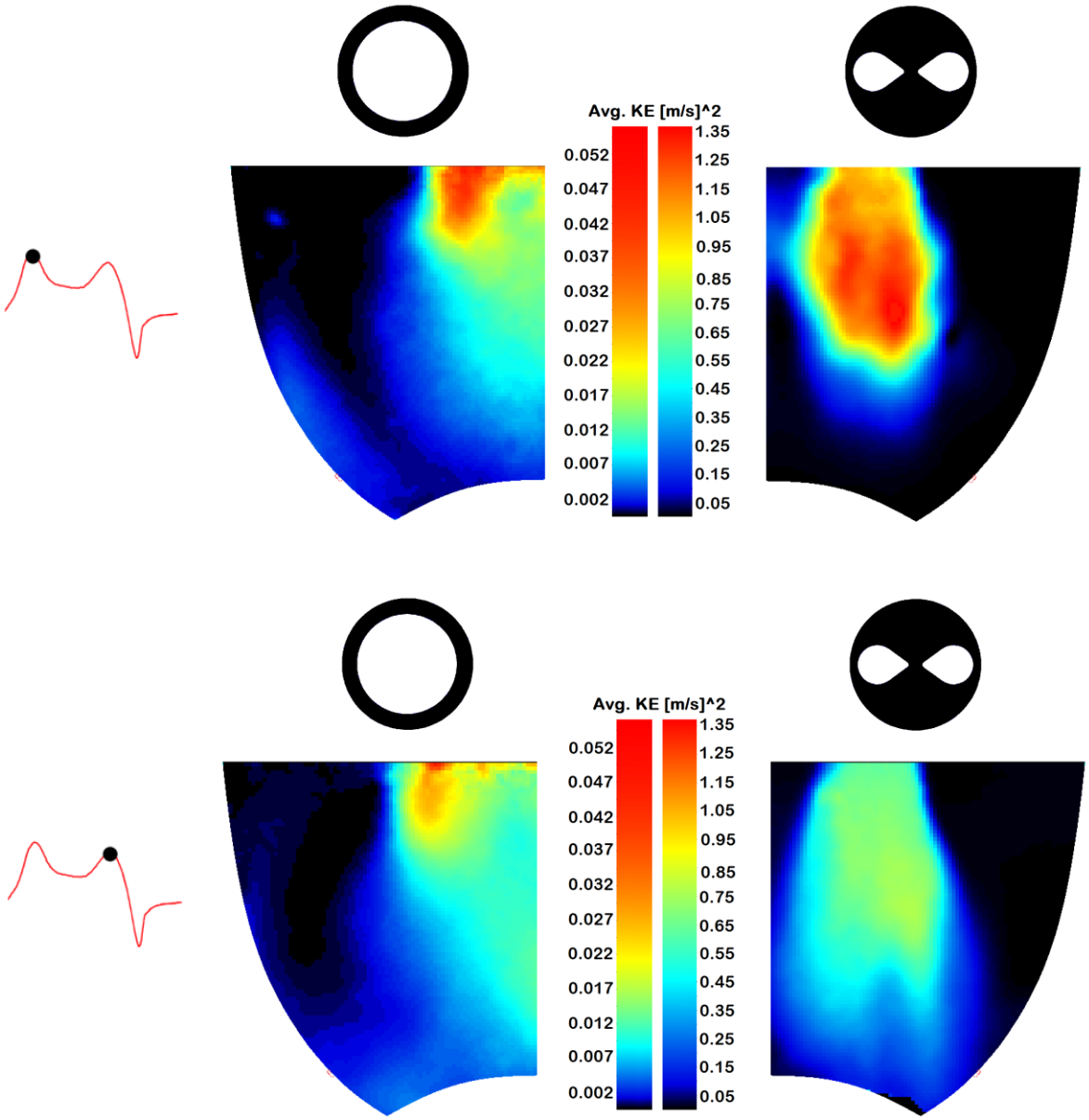

Figure 3-11: *Average kinetic energy at peak E and A waves for mitral regurgitation case and percutaneous edge-to-edge case.*

Such maps show that most of the kinetic energy is concentrated in the inflow jet region. Interestingly, the case simulating percutaneous EtER displays significant regions in the

flow field where the kinetic energy is almost zero. Such regions might predispose for thrombus formation.

Figure 3.12 represents the evolution of total kinetic energy, spatially averaged, for both cases investigated in this study, at eight different phases.

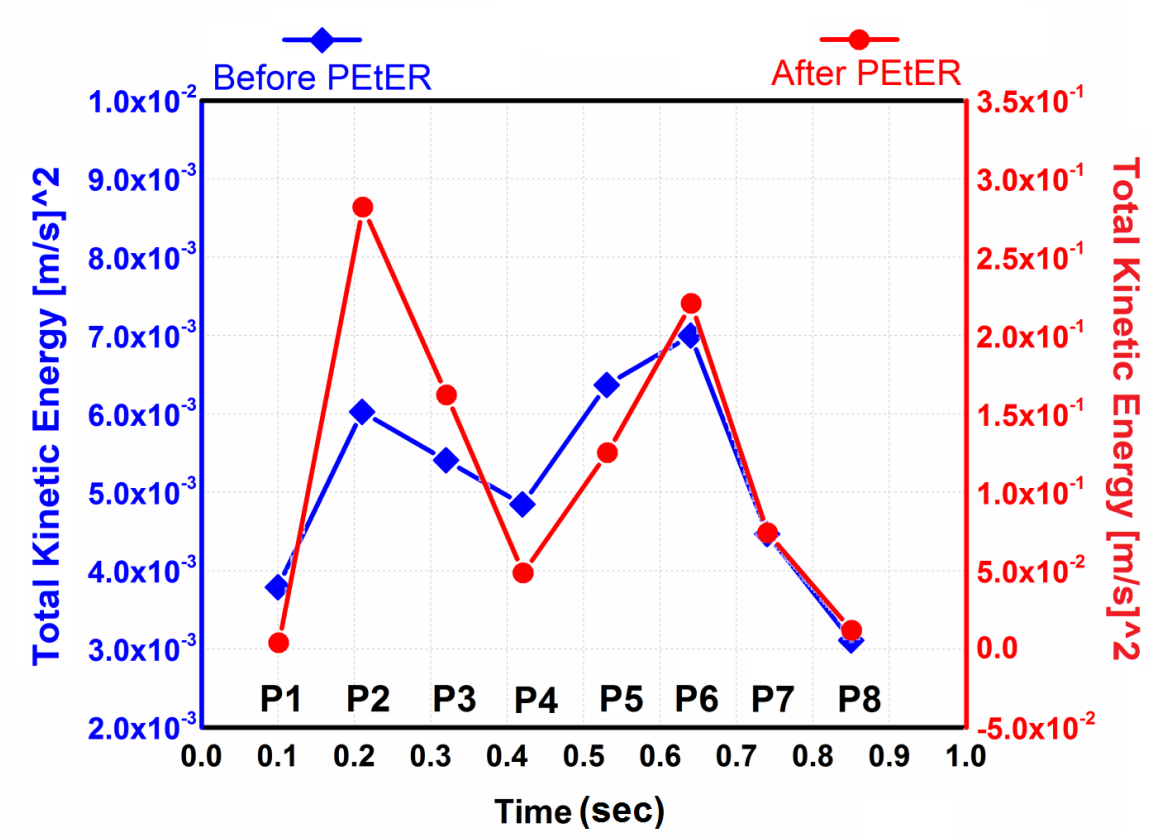

Figure 3-12: *Total kinetic energy for the seven different instants during diastole and one instant during systole. This figure scaled differently for two cases (the different instants correspond to the different phases as illustrated on figure 2-11).*

Although the trend for total kinetic energy between mitral regurgitation and following percutaneous edge-to-edge repair is not significantly different, the amplitude for percutaneous edge-to-edge repair is around two times of magnitude higher than for mitral

regurgitation. This means that left ventricle filling, following edge-to-edge repair, is performed at higher energetic cost.

Another interesting flow parameter to evaluate is the viscous dissipation of energy (Graw, et al. 2002):

$$\varepsilon = \mu \Delta A \sum_{x,y} 2\left[\left(\frac{du}{dx}\right)^2 + \left(\frac{dv}{dy}\right)^2\right] + \left(\frac{du}{dy} + \frac{dv}{dx}\right)^2 \qquad (Eq.\ 3.2)$$

where μ represents the dynamic viscosity of the fluid, ΔA stands for the interrogation area, u is the velocity component in the x-direction and v is the velocity component in the y-direction; dx and dy are the spatial resolutions in the x and y directions, respectively. Table 3.2 shows the difference in viscous dissipation at each phase between mitral regurgitation and percutaneous EtER. Increase in viscous dissipation of energy may lead a less efficient ventricular pumping function. Furthermore, less energy can be stored in the left ventricle during diastole and available for early systolic phase.

Table 3-2: *Representative of viscous dissipation of energy for different instants with the unit of Pa/s.*

	MR	PEtER
P1	3.63×10^{-3}	0.365×10^{-2}
P2	6.04×10^{-3}	29.80×10^{-2}
P3	5.02×10^{-3}	17.55×10^{-2}
P4	4.40×10^{-3}	4.98×10^{-2}
P5	6.24×10^{-3}	16.76×10^{-2}
P6	6.11×10^{-3}	27.48×10^{-2}
P7	5.00×10^{-3}	8.92×10^{-2}
P8	4.68×10^{-3}	2.43×10^{-2}

3.3.1.4 Reynolds Shear Stress

Reynolds Shear Stress (RSS) is averaged over 200 cycles. The assessment of RSS helps predicting the risk for shear induced blood components damage. This damage can be caused by prolonged collision and conflict of blood components, including the collision of red blood cells and platelets between each other, or the surface of the valve (Kheradvar et al. 2012). The regions with the potential of high Reynolds shear stresses may lead to hemolysis and platelets activation (Kameneva et al., 2004).

The RSS is calculated based on the velocity fields obtained from PIV measurements. RSS is not fixed by the rotation of the coordinate, so the major Reynolds stresses are

calculated along the principal axes (Baldwin et al. 1993). RSS (Eq. 3.4) and Reynolds normal stress (Eq. 3.5 and Eq. 3.6) are computed according to:

$$\overline{\rho uv} = \frac{1}{N}\sum_{i=1}^{N} \rho \acute{u}\acute{v} \qquad (Eq. 3.3)$$

$$\overline{\rho uu} = \frac{1}{N}\sum_{i=1}^{N} \rho \acute{u}^2 \qquad (Eq. 3.4)$$

$$\overline{\rho vv} = \frac{1}{N}\sum_{i=1}^{N} \rho \acute{v}^2 \qquad (Eq. 3.5)$$

N represents the number of images taken at each phase. Each velocity vector is decomposed into its mean component and its fluctuating velocity. So, $\acute{u}$ and $\acute{v}$ are fluctuating components of a velocity vector in x-direction and y-direction, respectively.

The major RSS is computed as:

$$RSS = (\left[\frac{\overline{\rho uu} - \overline{\rho vv}}{2}\right]^2 + \overline{\rho uv})^{\frac{1}{2}} \quad (Eq. 3.6)$$

Figure 3.13 shows the RSS field at the peak of E-wave and A-wave. Edge-to-edge repair induces significantly higher shear stress with maximal values of 4.4×10^{-2} $(m/s)^2$ at the peak of E-wave and 2.2×10^{-2} $(m/s)^2$ at the peak of A-wave. While, for the case with mitral regurgitation, the values were: 0.47×10^{-2} $(m/s)^2$, at the peak of E-wave and 0.15×10^{-2} $(m/s)^2$ at the peak of A-wave. These figures also show that edge-to-edge repair creates high shear stress layers that might damage red blood cells, or activate platelets with risks of hemolysis, or thrombus formation in the LV. Interestingly, Orban et al. (2012) have

already reported a case of thrombus formation in the LV following a successful percutaneous edge-to-edge repair.

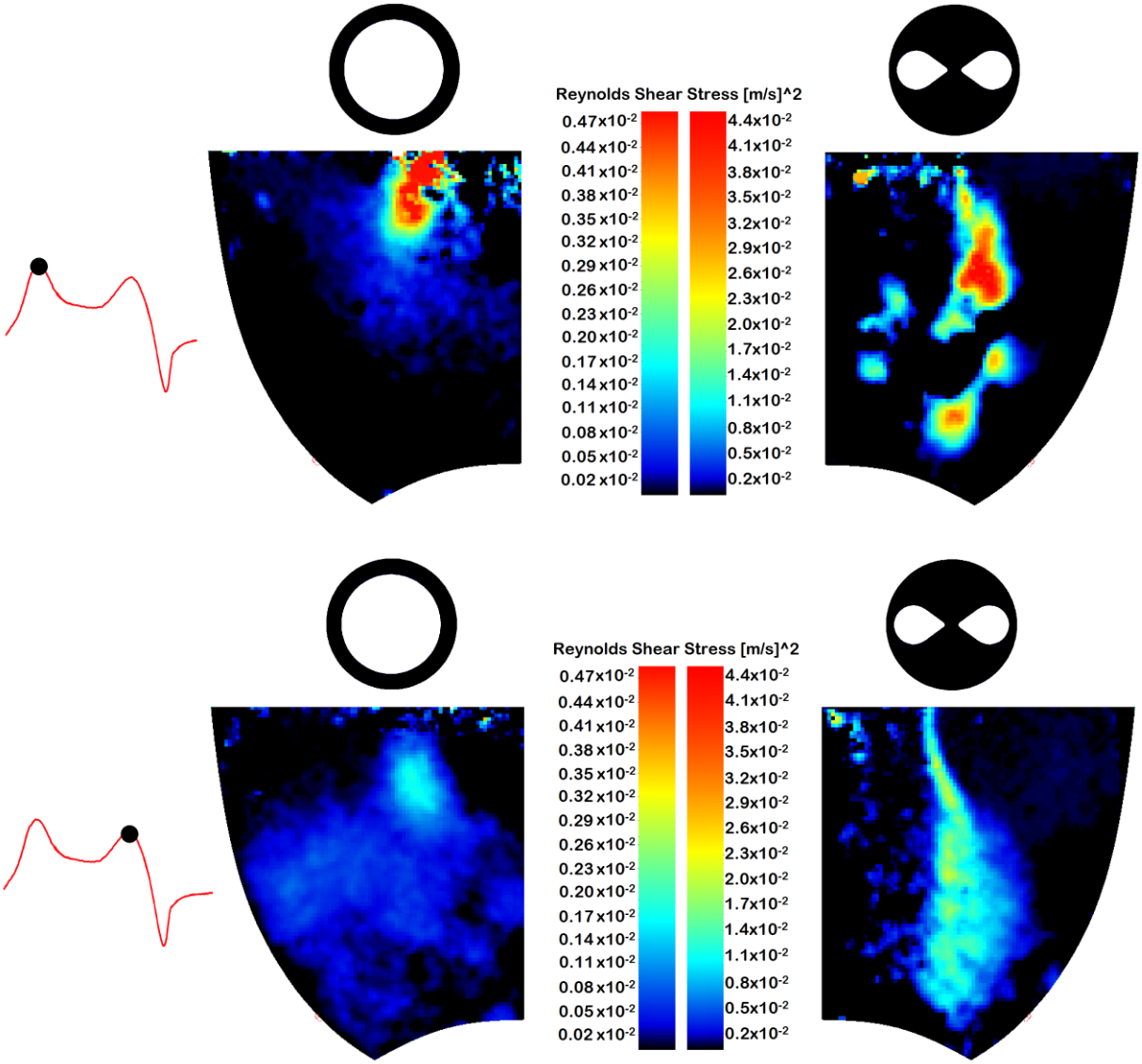

Figure 3-13: *Reynolds shear stress at the peak of E and A waves for MR and percutaneous EtER cases inside the LV.*

3.3.2 Time-Resolved Measurement

Time-resolved particle image velocimetry measurements were also performed in order to investigate flow dynamics in the left ventricle in the case of mitral regurgitation and following percutaneous edge-to-edge repair. Of interest here is the evolution of the vorticity field during left ventricle filling phase. Other results, including velocity fields and viscous energy dissipation derived from time-resolved measurements can be found in Appendix.

3.3.2.1 Vortex Dynamics inside the Left Ventricle

Figure 3.14 represents the vorticity field at four instants during left ventricle filling phase. The maximum of vorticity is 320 s^{-1}. Dispersed small scale coherent structures can be noticed in the flow field.

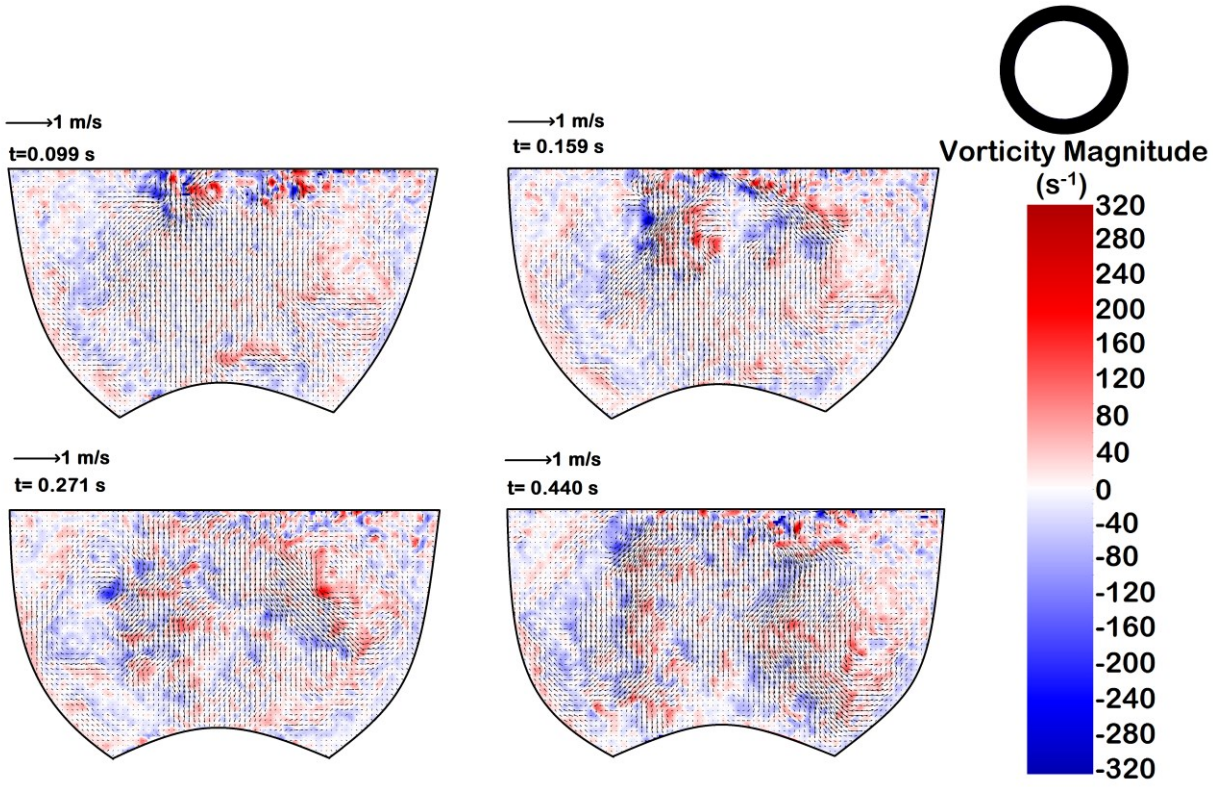

Figure 3-14: *Vorticity magnitude for t=0.099 s, t=0.159 s, t=0.271 s and t=0.440 s for the MR case.*

The trend is significantly different for the case with percutaneous edge-to-edge repair. The vorticity magnitude is significantly higher than for the mitral regurgitation case and reaches a maximum of 1800 s^{-1}. A vortex ring is formed early in diastole and is rapidly convected towards the apex. At instant t=0.165 s, a vortical structure can also be observed between the two jets emerging from each orifice of the repaired mitral valve (Figure 3.15).

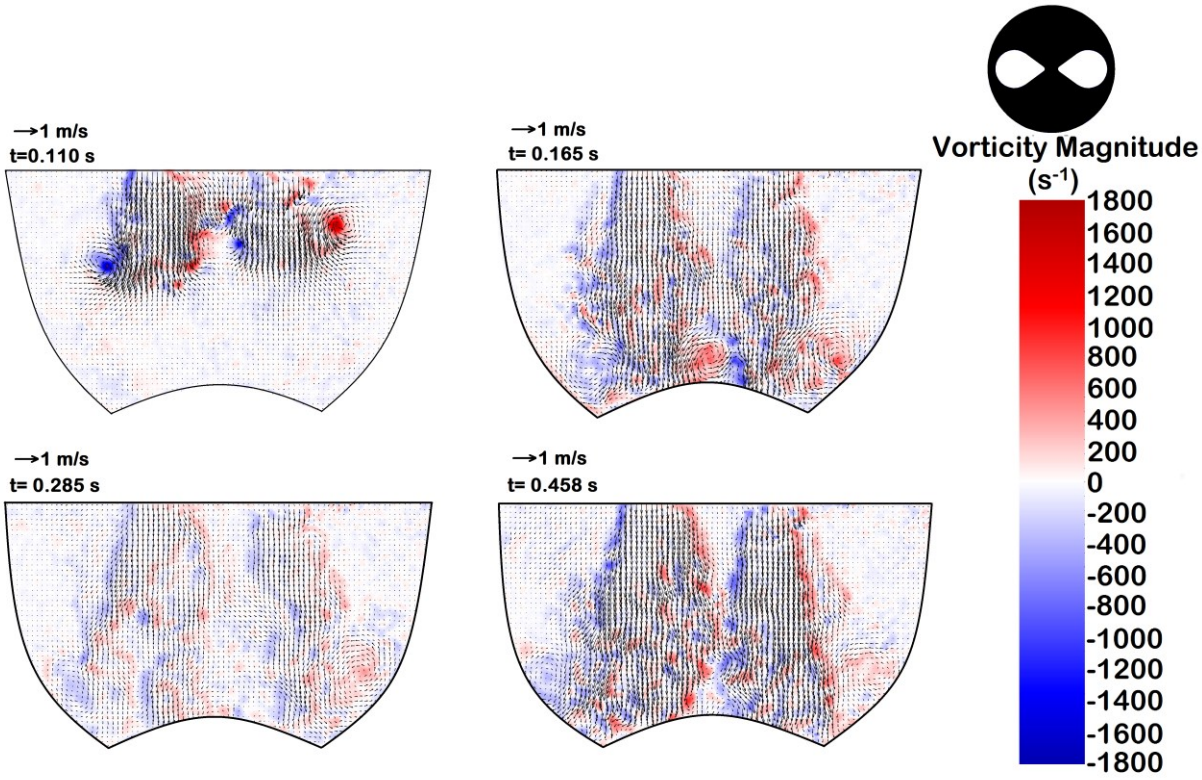

Figure 3-15: *Vorticity magnitude for t=0.110 s, t=0.165 s, t=0.285 s and t=0.458 s for the EtER case.*

Time resolved measurements allow for the evaluation of speed at which coherent structures are convected into the LV during one cycle and mainly during early diastolic phase (E-wave). For this, a space-time plot is represented for each case investigated in this work. For this purpose, the time evolution of the axial velocity along a line passing through the mitral orifice (one of the two orifices for the case with percutaneous edge-to-edge repair) is plotted. Then, the location of the maximal velocity along the line is obtained at each instant and a linear regression allows for the estimation of the speed of the propagation of the vortex structures in the left ventricle.

Below figures represent the space-time velocity distribution during E-wave. In these figures the slope of dashed line shows the propagation of the vortices for MR case; the estimated propagation velocity is 15 mm/s (Figure 3.16). For EtER case the propagation velocity is significantly higher and reaches 99 mm/s (Figure 3.17).

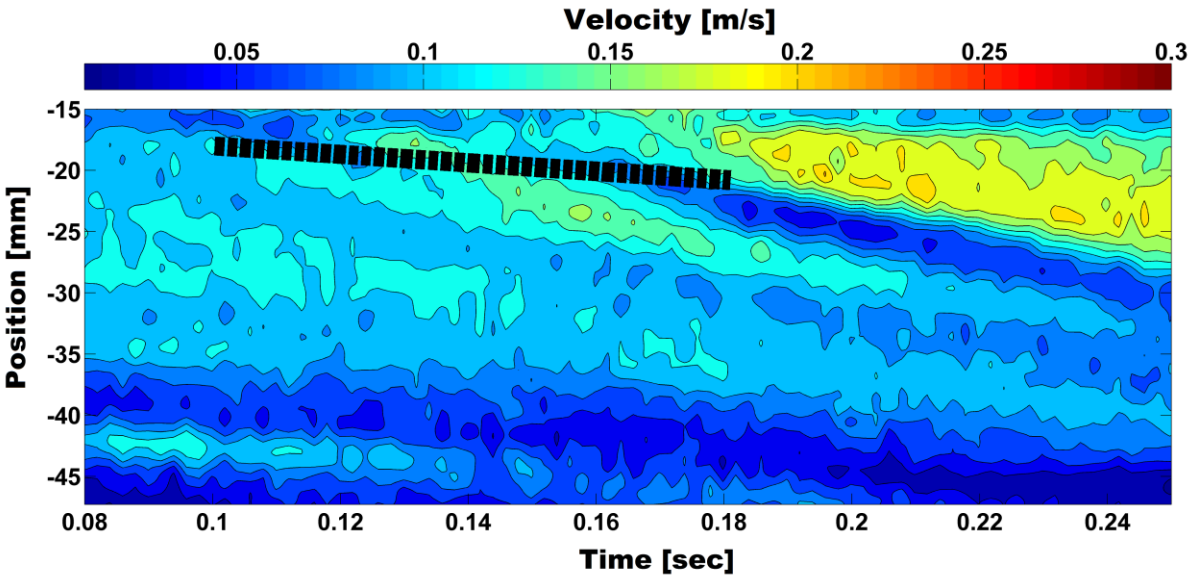

Figure 3-16: *Space-time velocity of E-Wave for the MR case.*

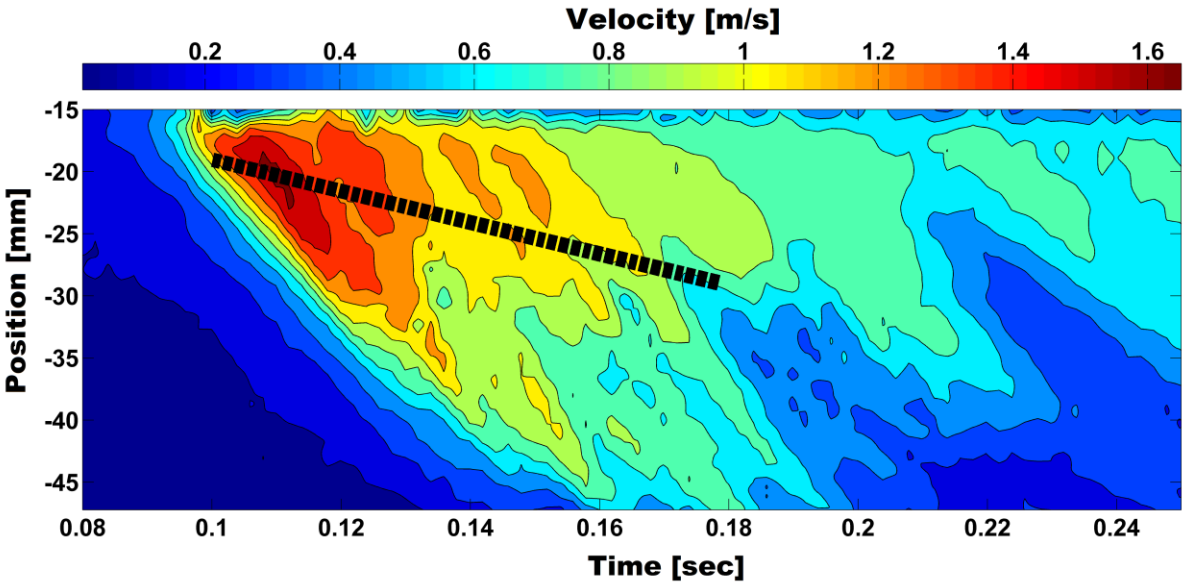

Figure 3-17: *Space-time velocity of E-Wave for the EtER case.*

Chapter 4 : Conclusion and Future Works

The key findings of this study are: 1) there was a good agreement between Doppler and catheter transvalvular pressure measurements in the case of double orifice MV configuration; 2) Percutaneous EtER significantly modified flow patterns and vortex dynamics in the LV.

Recent studies have shown that about half of the patients with symptomatic severe MR are not referred to surgery mainly because of age or the presence of comorbidities (Van den Branden et al., 2007). For such patient, percutaneous EtER using MitraClip appears as a viable solution. EVEREST I (Endovascular Valve EtER Study I) demonstrated mainly the safety and feasibility of the MitraClip. However, the results from EVEREST II on 179 patients have shown that percutaneous EtER does not outperform surgery in symptomatic patients with MR. Although the number of major adverse events was significantly lower in patients with a MitraClip, the rate of surgery/reoperation was significantly higher compared to the surgical group (Munkholm-Larsen et al., 2013). As a consequence, the recent guidelines from the European Society of Cardiology and the European Association for Cardio-Thoracic Surgery suggest that MitraClip has been used in high surgical risk patients and considered by a multidisciplinary team.

4.1 Hemodynamic Performance Following Percutaneous EtER

The double orifice configuration generated by EtER poses challenges for the evaluation of MV function. In this study, we showed that there was a good agreement between the maximal velocity measured by Doppler and PIV (1.60 m/s *vs.*1.58 m/s). Furthermore, we found a good match between Doppler and catheter transmitral pressure gradients (Peak TMPG: 9 mmHg *vs.* Catheter: 7 mmHg; Mean TMPG: 4 mmHg vs. 3 mmHg). The values for TPMG obtained in this study are in good agreement with *in vivo* data from the literature. In 84 patients with EtER, Hilberath et al. (2013) found a peak TMPG of 10.7±0.5 mmHg and a mean TMPG of 4.3±0.2 mmHg, while Hermann et al. (2009) reported a mean TMPG of 4.1±2.2, and Divchev et al. a mean TMPG of 3.6±1.5 mmHg.

4.1.1 Location of Doppler Measurements

Maisano et al. (2000) showed numerically that up to 35% can be obtained in the estimation of TMPG depending on the location of the measurements. In this study, we found even larger difference between the jet velocity and the central line velocity. At the peak of the E-wave, the jet velocity was around three times higher than the central line velocity, while at the peak of the A-wave, the jet velocity was about six times higher. Alignment of the Doppler probe is therefore essential in order to limit measurement errors. Another finding was that the jet velocity remained at its maximal value for around two orifice diameters (around 20 mm). As a result, if pulsed Doppler is

used to evaluate MV function following EtER, the results are less affected by the longitudinal positioning of the probe inside the LV.

4.1.2 Flow Patterns in the LV Following Percutaneous EtER

The results of this study showed significant modifications in flow patterns in the LV following EtER. Except for the development of a double jet configuration, the vortex structures in the LV were significantly different from a normal LV filling. EtER generated smaller vortex structures that were rapidly convected towards the apex and significantly contributed in dissipating flow energy. This energy lost as heat is not available during LV systole to transport blood flow through the arterial system. These findings are in agreement with the results obtained numerically by Hu et al. (2010).

4.2 Future Works

Left human heart ventricle is one of the most sophisticated parts in cardiovascular system from the hemodynamics and fluid mechanics point of view.

In this *in vitro* study, blood flow behavior under pathological condition after valve edge-to-edge repair was investigated. This experimental study revealed interesting results regarding the flow behavior inside the LV. However, future studies performed using 3D stereoscopic PIV should be performed in order to more accurately investigate the flow in the LV following edge-to-edge repair.

Also from a fluid mechanics point-of-view, vortex formation and reconnection for flow conditions mimicking percutaneous edge-to-edge repair will be an interesting area to investigate.

Finally, from a clinical point-of-view the effect of mitral valve area reduction following edge-to-edge repair on left atrium pressure and pulmonary hypertension has to investigate.

References

Books and Articles

- B. J. L. Van den Branden, M. J. Swaans, M. C. Post, B. J. W. M. Rensing, F. D. Eefting, W. Jaarsma, and J. S. Van der Heyden, "Percutaneous edge-to-edge mitral valve repair in high-surgical-risk patients: do we hit the target?," *J. Am. Coll. Cardiol. Intev.*, vol. 5, no. 1, pp. 105–111, Jan. 2012.

- C. Fucci, L. Sandrelli, A. Pardini, L. Torracca, and M. Ferrari, "Improved results with mitral valve repair using new surgical techniques," *Eur. J. Cardio-thorac Surg.,* , pp. 621–627, 1995, Jan. 1987.

- D. Divchev, S. Kische, L. Paranskaya, H. Schneider, T. Rehders, J. Ortak, I. Akin, G. Turan, C. H. Turan, G. Steinhoff, G. Nöldge-Schomburg, C. Nienaber, and H. Ince, "In-hospital outcome of patients with severe mitral valve regurgitation classified as inoperable and treated with the MitraClip® device," *J. Interv. Cardiol.*, vol. 25, no. 2, pp. 180–189, Apr. 2012.

- D. H. Adams, and F. Filsoufi, "Another chapter in an enlarging book: repair degenerative mitral valves," *J. Thorac. Cardiovasc. Surg*., vol. 125, no. 6, pp. 1197–1199, Jun. 2003.

- F. Maisano, A. Redaelli, G. Pennati, R. Fumero, L. Torracca, and O. Alfieri, "The hemodynamic effects of double-orifice valve repair for mitral regurgitation: a 3D computational model," *Eur. J. Cardiothorac. Surg.*, vol. 15, no. 4, pp. 419–425, Apr. 1999.

- F. Maisano, J. J. Schreuder, M. Oppizzi, B. Fiorani, C. Fino, and O. Alfieri, "The double-orifice technique as a standardized approach to treat mitral regurgitation due to severe myxomatous disease: surgical technique," *Eur. J. Cardiothorac. Surg.*, vol. 17, no. 3, pp. 201–205, Mar. 2000.

- G. Pedrizzetti, and F. Domenichini, "Nature optimizes the swirling flow in the human left ventricle," *Phys. Rev. Lett.*, vol. 95, no. 10, pp. 1–4, Sep. 2005.

- G. Hong, G. Pedrizzetti, G. Tonti, P. Li, Z. Wei, J. K. Kim, A. Baweja, S. Liu, N. Chung, H. Houle, J. Narula, and M. Vannan, "Characterization and quantification of vortex flow in the human left ventricle by contrast echocardiography using vector particle image velocimetry.," *J. Am. Coll. Cardiol. Img.*, vol. 1, no. 6, pp. 705–717, Nov. 2008.

- H. Herrmann, S. Kar, R. Siegel, P. Fail, C. Loghin, S. Lim, R. Hahn, J. Rogers, W. Bommer, A. Wang, Berke A, S. Lerakis, P. Kramer, S, Wong, E. Foster, D. Glower, and T. Feldman, "Effect of percutaneous mitral repair with the MitraClip device on mitral valve area and gradient," *EuroIntervention*, 4 pp. 437–442, Jan. 2009.

- J. H. Rogers, and O. Franzen, “Percutaneous edge-to-edge MitraClip therapy in the management of mitral regurgitation,” *Eur. Heart J.*, vol. 32, no. 19, pp. 2350–2357, Oct. 2011.

- J. N. Hilberath, H. K. Eltzschig, S. K. Shernan, A. H. Worthington, S. F. Aranki, and M. Nowak-Machen, “Intraoperative evaluation of transmitral pressure gradients after edge-to-edge mitral valve repair,” *PLoS One*, vol. 8, no. 9, pp. e73617, Jan. 2013.

- J. Rogers, O. Franzen, and S. F. Bolling, “Atlas of percutaneous edge-to-edge mitral valve repair: mitral valve anatomy and current surgical and percutaneous approaches to mitral regurgitation,” *Springer*, pp. 1–11, 2013.

- J. T. Baldwin, S. Deutsch, J. M. Tarbell, and H. L. Petrie, “Determination of principal reynolds stresses in pulsatile flows after elliptical filtering of discrete velocity measurements,” *J. Biomech. Eng.*, vol. 115, no. 4A, pp. 396–403, Nov. 1993.

- J. Westerweel, “Fundamentals of digital particle image velocimetry,” *Meas. Sci. Technol.*, vol. 8, no. 12, pp. 1379–1392, Dec. 1997.

- K. Graw, and J. Lengricht, "Particle Image Velocimetry (PIV) in coastal engineering," *1st German-Chinese Joint Symposium on Coastal and Ocean Engineering (Joint 2002),* 10-14 April 2002.

- K.B. Chandran, R. Schoephoerster, and K.C. Dellsperger, "Effect of prosthetic mitral valve geometry and orientation on flow dynamics in a model human left ventricle," *J. Biomech.*, vol. 22, no. 1, pp. 51-65, 1989.

- A. Kheradvar, and G. Pedrizzetti, "Vortex formation in the cardiovascular system," *Springer London*, 2012.

- L. J. Olson, R. Subramanian, D. M. Ackermann, T. A. Orszulak, and W. D. Edwards, "Surgical pathology of the mitral valve: a study of 712 cases spanning 21 years," *Mayo Clin. Proc.*, vol. 62, no. 1, pp. 22–34, Jan. 1987.

- L. M. Bakker, M. J. Swaans, J. S. van der Heyden, F. D. Eefting, B. J. W. M. Rensing, and M. C. Post, "Complications during percutaneous edge-to-edge mitral valve repair," *Herz*, no. 38, pp. 484–489, Jun. 2013.

- M. Calafiore, M. Di Mauro, M. Contini, L. Weltert, and A. Bivona, "Mitral valve repair in ischemic mitral regurgitation," *Multimed. Man. Cardio-Thoracic Surg.*, vol. 2005, no. 0324, pp. 1–5, Jan. 2005.

- M. Daimon, G. Saracino, M. Gillinov, Y. Koyama, S. Fukuda, J. Kwan, J. Song, V. Kongsaerepong, D. Agler, J. D. Thomas, and T. Shiota, "Local dysfunction and asymmetrical deformation of mitral annular geometry in ischemic mitral regurgitation: a novel computerized 3D echocardiographic analysis," *Echocardiography*, vol. 25, no. 4, pp. 414–423, Apr. 2008.

- M. Gillinov, C. Faber, P. L. Houghtaling, E. H. Blackstone, B. Lam, R. Diaz, B. W. Lytle, J. F. Sabik, and D. M. Cosgrove, "Repair versus replacement for degenerative mitral valve disease with coexisting ischemic heart disease," *J. Thorac. Cardiovasc. Surg.*, vol. 125, no. 6, pp. 1350–1361, Jun. 2003.

- M. Gillinov, E. H. Blackstone, E. R. Nowicki, W. Slisatkorn, G. Al-Dossari, D. R. Johnston, K. M. George, P. L. Houghtaling, B. Griffin, J. F. Sabik, and L. G. Svensson, "Valve repair versus valve replacement for degenerative mitral valve disease," *J. Thorac. Cardiovasc. Surg.*, vol. 135, no. 4, pp. 885–893, 893.e1–2, Apr. 2008.

- M. Mirabel, B. Iung, G. Baron, D. Messika-Zeitoun, D. Détaint, J.-L. Vanoverschelde, E. G. Butchart, P. Ravaud, and A. Vahanian, "What are the characteristics of patients with severe, symptomatic, mitral regurgitation who are denied surgery?," *Eur. Heart J.*, vol. 28, no. 11, pp. 1358–1365, Jun. 2007.

- M. Orban, H. Lesevic, S. Massberg, and J. Hausleiter, “Left ventricular thrombus formation after successful percutaneous edge-to-edge mitral valve repair,” *Eur. Heart J.*, vol. 34, pp. 942, Aug. 2012.

- M. Raffel, C. E. Willert, S. T. Wereley, and J. Kompenhans. “Particle image velocimetry: a practical guide,” *Springer*. 2004.

- N. C. Dang, M. S. Aboodi, T. Sakaguchi, H. S. Wasserman, M. Argenziano, D. M. Cosgrove, T. K. Rosengart, T. Feldman, P. C. Block, and M. C. Oz, “Surgical revision after percutaneous mitral valve repair with a clip: initial multicenter experience,” *Ann. Thorac. Surg.*, vol. 80, no. 6, pp. 2338–2342, Dec. 2005.

- N. M. Van Mieghem, N. Piazza, R. H. Anderson, A. Tzikas, K. Nieman, L. De Laat, J. S. McGhie, M. L. Geleijnse, T. Feldman, P. W. Serruys, and P. Jaegere, “Anatomy of the mitral valvular complex and its implications for transcatheter interventions for mitral regurgitation,” *J. Am. Coll. Cardiol.*, vol. 56, no. 8, pp. 617–626, Aug. 2010.

- O. Alfieri, F. Maisano, and M. De Bonis, “The edge-to-edge repair,” *Multimed. Man. Cardio-Thoracic Surg.*, vol. 2005 , no. 0809 , Jan. 2005.

- O. Alfieri, F. Maisano, M. De Bonis, P. L. Stefano, L. Torracca, M. Oppizzi, and G. La Canna, "The double-orifice technique in mitral valve repair: a simple solution for complex problems," *J. Thorac. Cardiovasc. Surg.*, vol. 122, no. 4, pp. 674–681, Oct. 2001.

- P. H. Loh, K. T. Veien, O. Gaemperli, and R. Corti, "Atlas of percutaneous edge-to-edge mitral valve repair," *Springer* pp. 147–162, 2013.

- P. Lancellotti, C. Tribouilloy, A. Hagendorff, L. Moura, B. Popescu, E. Agricola, J.-L. Monin, L. Pierard, L. Badano, and J. L. Zamorano, "European Association of Echocardiography recommendations for the assessment of valvular regurgitation. Part 1: aortic and pulmonary regurgitation (native valve disease)," *Eur. J. Echocardiogr.*, vol. 11, no. 3, pp. 223–244, Apr. 2010.

- P. O'Gara, L. Sugeng, R. Lang, M. Sarano, J. Hung, S. Raman, G. Fischer, B. Carabello, D. Adams, and M. Vannan, "The role of imaging in chronic degenerative mitral regurgitation," *J. Am. Coll. Cardiol. Img.*, vol. 1, no. 2, pp. 221–237, Mar. 2008.

- R. Estévez-Loureiro, O. Franzen, R. Winter, L. Sondergaard, P. Jacobsen, G. Cheung, N. Moat, N. Ihlemann, M. Ghione, S. Price, A. Duncan, T. S. Rosenberg, S. Barker, C. Mario, and M. Settergren, "Echocardiographic and clinical outcomes of central versus non-central percutaneous edge-to-edge repair of degenerative mitral regurgitation," *J. Am. Coll. Cardiol.*, Aug. 2013.

- S. Munkholm-Larsen, B. Wan, D. H. Tian, K. Kearney, M. Rahnavardi, U. Dixen, L. Køber, O. Alfieri, and T. D. Yan, "A systematic review on the safety and efficacy of percutaneous edge-to-edge mitral valve repair with the MitraClip system for high surgical risk candidates," *Heart.* , Jun. 2013.

- T. Schenkel, and H. Oertel, "Numerical simulation of the asymmetric redirection of blood flow in the left ventricle," *J. Biomech.*, vol. 39, pp. S310, 2006.

- V. T. Nkomo, J. M. Gardin, T. N. Skelton, J. S. Gottdiener, C. G. Scott, and M. Enriquez-Sarano, "Burden of valvular heart diseases: a population-based study," *Lancet*, vol. 368, no. 9540, pp. 1005–1011, Sep. 2006.

- W. Nichols, M. F. O'Rourke, and Ch. Valchopoulos "McDonald's blood flow in arteries," *UK: Hooder Arnolds*, 2011.

- W. R. E. Jamieson, F. H. Edwards, M. Schwartz, J. W. Bero, R. E. Clark, and F. L. Grover, "Risk stratification for cardiac valve replacement. National Cardiac Surgery Database," *Ann. Thorac. Surg.*, vol. 67, no. 4, pp. 943–951, Apr. 1999.

- W. Schiller, T. Schmid, K. Spiegel, S. Donisi, C. Probst, A. Kovacz, S. Flacke, D. Liepsch, and H. Oertel, "Computational simulation of blood flow in the human left ventricle," *J. Biomech.*, vol. 39, pp. S297, 2006.

- Y. Hu, L. Shi, S. Parameswaran, S. Smirnov, and Z. He, "Left ventricular vortex under mitral valve edge-to-edge repair," *Cardiovasc. Eng. Technol.*, vol. 1, no. 4, pp. 235–243, Dec. 2010.

Websites

- Mitral Valve Repair Center (March 2013): https://www.mitralvalverepair.org
- Mitral Valve (March 2013): https://www.themitralvalve.org
- The Cardio-Thoracic Surgery Network (March 2013): https://www. ctsnet.org
- National Heart, Lung, and Blood Institute (March 2013): https://www. nhlbi.nih.gov
- www.dantecdynamics.com

Technical Manuals

- ViVitro Operating Manual. ViVitro System Inc., 2006, Victoria, Canada.

Appendix

Viscous Dissipation of Energy

In a viscous fluid flow the viscosity of the fluid will take energy from the kinetic of fluid and transform it to the internal energy (heat). This irreversible process named viscous dissipation. In order to calculate the Viscous Dissipation of Energy respect to the previous equation we have:

$$\varepsilon = \mu \Delta A \sum_{x,y} 2\left[\left(\frac{du}{dx}\right)^2 + \left(\frac{dv}{dy}\right)^2\right] + \left(\frac{du}{dy} + \frac{dv}{dx}\right)^2 \qquad (Eq.A.1)$$

Where μ is representing the dynamic viscosity of the fluid. dx and dy are spacing between velocity vectors. This equation (Eq. A.1) obtained from (Graw, et al. 2002).

Below graph represents the viscous dissipation of energy in systole and diastole of the LV before intervention as MR case. This graph discloses how the viscosity of the fluid during the cardiac cycle took energy from the kinetic energy (motion) of the fluid and transforms it to the irreversible internal energy. During the cardiac cycle it changes around 0.02 Pa/sec and as it is unfolded for two critical moments of each cardiac cycle, E-Wave and A-Wave, the changes was not enormous and viscous dissipations were smooth and argumentative.

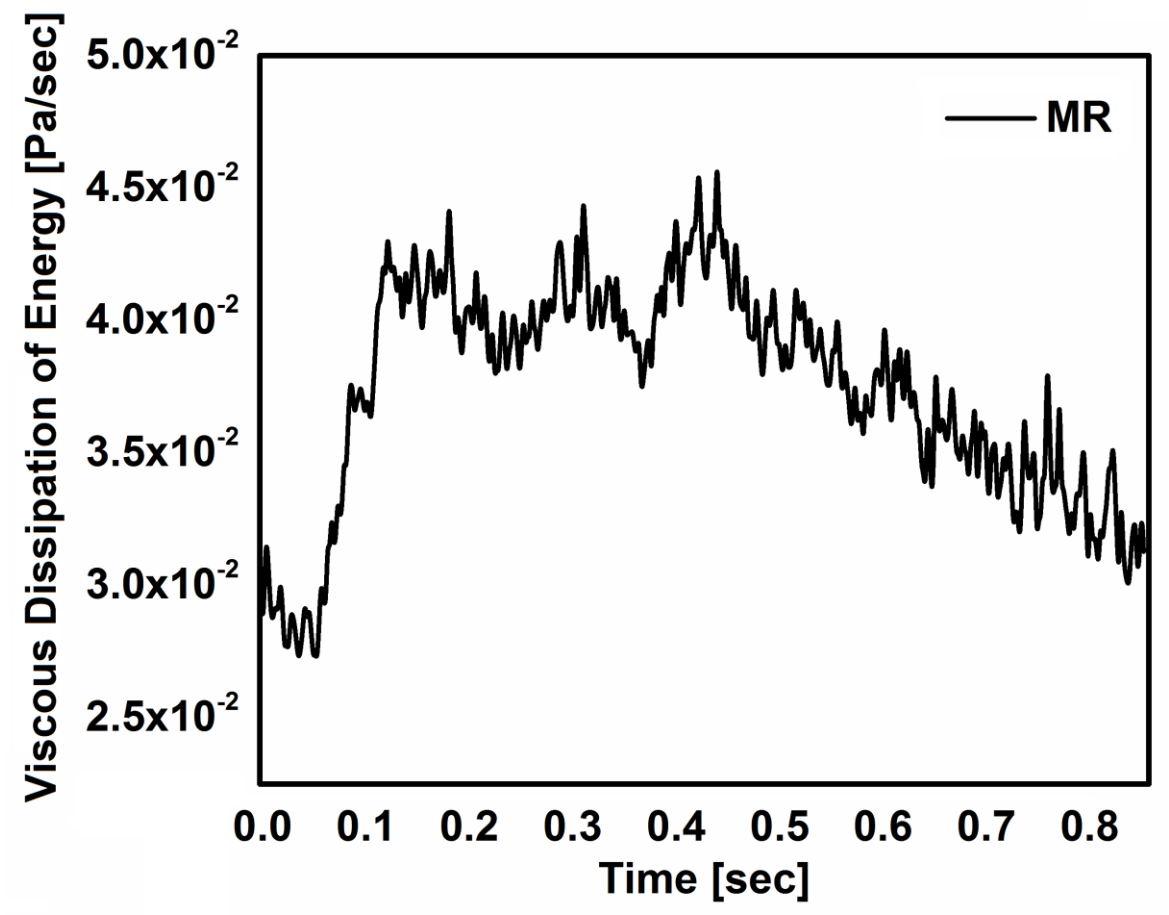

Figure A-1: *Viscous dissipation of energy for MR case in one cardiac cycle.*

Figure A.2 illustrates viscous dissipation for the cardiac cycle after simulating the percutaneous EtER of mitral valve. This graph reveals the trend has changed completely and strongly asserts that how this operation has altered the blood flow inside the LV. The whole variation of the viscous dissipation is around 0.8 Pa/sec and this variation for the E-Wave and A-Wave in compare to the other moments of the cycle is around 63% to 87% that might endanger blood components and damage them. Also the variations during the cardiac cycle before and after the intervention are about 60% to 93%.

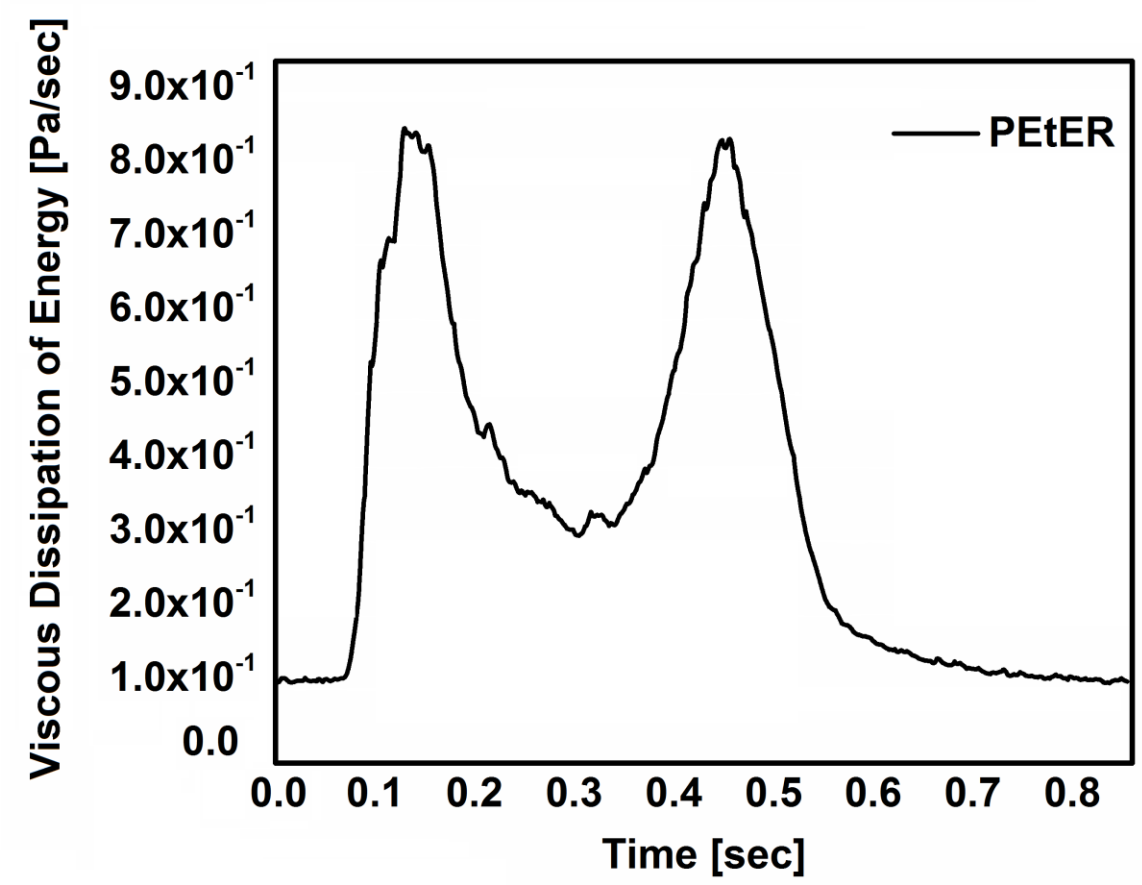

Figure A-2: *Viscous dissipation of energy for MR case in one cardiac cycle.*

Velocity Pattern

Figure A.3 represents the velocity magnitude for four different time of t=0.099, 0.159, 0.271 and 0.440 seconds in one cardiac cycle (Δt=0.857 s) for MR case. These moments respectively are stand for the peak and deceleration of E-Wave, diastasis and peak of A-Wave.

In all the mentioned instants distribution of the velocity magnitude is smooth and has changed for 0.3 m/s with higher rates along the ejected mitral jet. In t=0.099 s and t=0.440 s the higher velocity is distributed at the level of the valve.

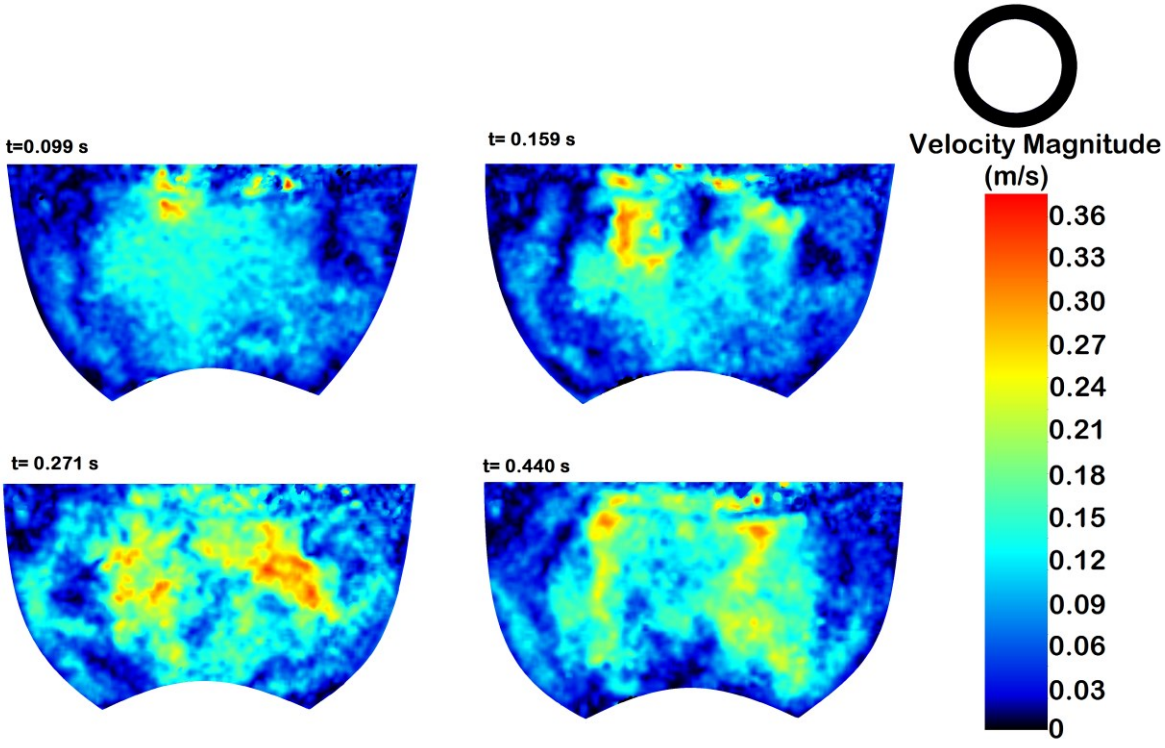

Figure A-3: *Velocity magnitude for t=0.099 s, t=0.159 s, t=0.271 s and t=0.440 s for the MR case.*

Figure A.4 roughly shows the same instants at the times of t=0.110, 0.165, 0.285 and 0.458 seconds. Contrary to the previous case the velocity pattern inside the LV is harsh and higher velocity sharply diffused along the jets with 60% to 70% difference by the value of very close neighbouring regions.

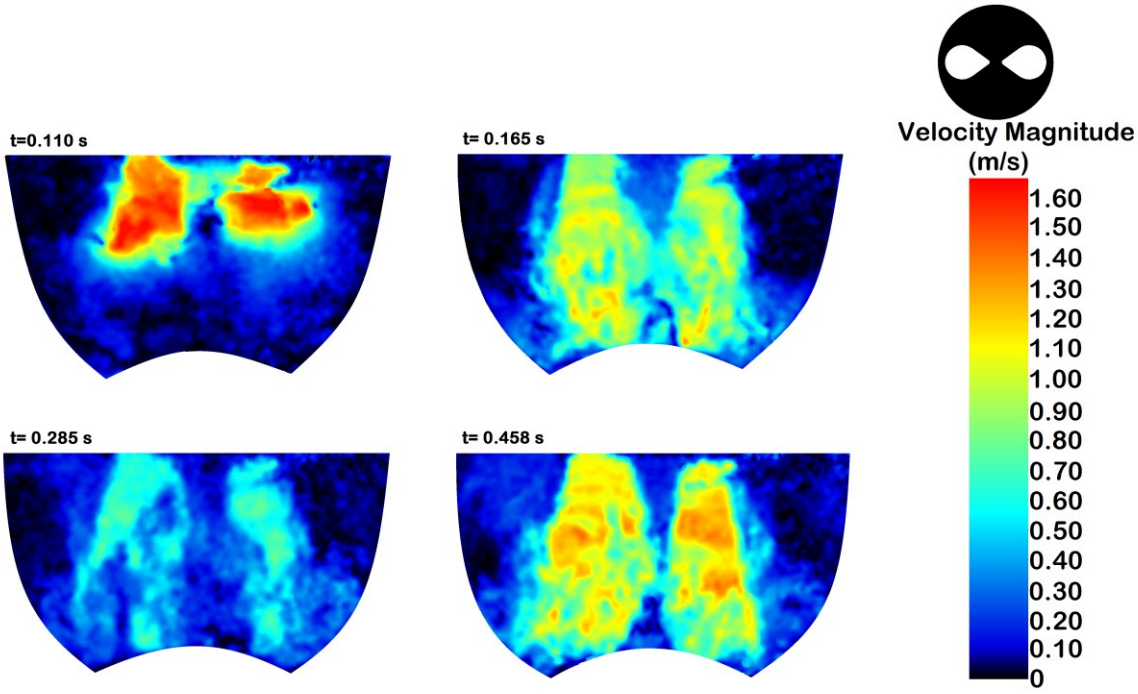

Figure A-4: *Velocity magnitude for t=0.110 s, t=0.165 s, t=0.285 s and t=0.458 s for the EtER case.*